CONSTRUCTING A GEOMECHANICAL MODEL OF THE WOODFORD SHALE,

CHEROKEE PLATFORM, OKLAHOMA, USA

EFFECTS OF CONFINING STRESS AND ROCK STRENGTH ON FLUID FLOW

By

TYLER J. HAIR

Bachelor of Science, 2010
Brigham Young University
Provo, Utah

Submitted to the Graduate Faculty of
The College of Science and Engineering
Texas Christian University
In partial fulfillment of the requirements for the degree of
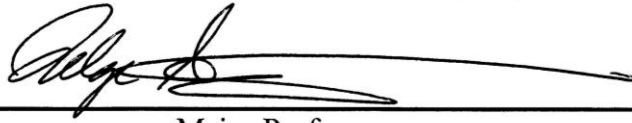

MASTER OF SCIENCE

August, 2012

CONSTRUCTING A GEOMECHANICAL MODEL OF THE WOODFORD SHALE,
CHEROKEE PLATFORM, OKLAHOMA, USA
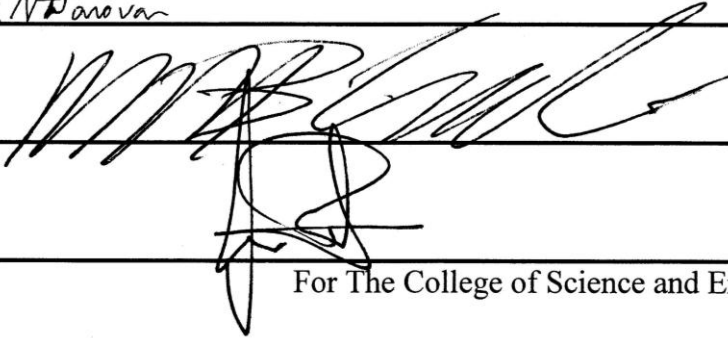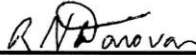EFFECTS OF CONFINING STRESS AND ROCK STRENGTH ON FLUID FLOW

By

TYLER J. HAIR

Thesis approved:

_____
Major Professor

_____

_____
For The College of Science and Engineering

ACKNOWLEDGEMENTS

LIST OF FIGURES

LIST OF TABLES

TABLE OF CONTENTS

Vita

Abstract

INTRODUCTION

A better understanding of the mechanical properties of drilled rock formations can alleviate many of the problems associated with drilling for and producing oil and gas from wells. Potential drilling and production problems include wellbore stability, sand production, changes in porosity and permeability due to compaction during reservoir depletion, closure of fracture apertures as a result of fluid production and lost circulation associated with the reactivation of planar mechanical discontinuities (Weingarten and Perkins, 1995; Khaksar et al., 2009; Enderlin and Alsleben, in press). One important mechanical property to understand in order to avoid these drilling problems is rock strength, which is defined herein as the level of stress at which failure occurs. Rock strength is a function of many components, including lithology, porosity, permeability, secondary chemical processes, the geospatial position of the rock within the modern-day stress field and the presence of inherent weaknesses (referred to herein as mechanical discontinuities) (Laubach et al., 2004; Khaksar et al., 2009; Enderlin and Alsleben, in press). Changes in the confining stress surrounding a rock can modify porosity and permeability as well as result in structural deformation through compaction, fracturing, faulting or folding. These changes alter the rock strength and influence fluid flow along planar mechanical discontinuities within the rock (Enderlin and Alsleben, in press).

Rock strength can be determined using a number of methods. Triaxial load cells use a combination of pistons, fluids, and impermeable jackets to apply a confining pressure on all sides of a cylindrical rock specimen. By varying the magnitude of stress applied from different directions, a wide array of failure conditions can be simulated to determine the strength of a rock (Van der Pluijm and Marshak, 2004). As an alternative to triaxial tests, rock strength may be obtained from formation evaluation well logs (e.g., Work, 1975; Fertl and Chilingarian, 1990;

Woehrl et al., 2010). This approach is advantageous because it allows for calculating a continuous succession of mechanical properties over a depth interval, and can expand the scope of a study area due to the greater availability of well logs (Woehrl et al., 2010). In addition, a number of empirical methods involving impacts and indentations on a sample surface have been used to measure the strength of a rock, including point load penetrometers of various shapes and sizes, Schmidt rebound hammers and the Los Angeles abrasion test (Cargill and Shakoor, 1990).

In this study, a micro-indentation method is applied to determine the rock strength of the Woodford Shale in a localized region on the Anadarko Shelf. Whole core collected from the EOG Smith, B. 31 #3 Saltwater Disposal (SWD) well has been analyzed using this method to construct a geomechanical model of the Woodford that enables one to predict and avoid the diversion of fluids. The Smith, B. 31 #3 is located in section 31 of township 14N range 2E, Lincoln County, Oklahoma, USA (Figure 1).

The strength of a rock maintains an equilibrium relationship with magnitudes of present-day stresses, insuring that when the stresses acting on a rock diverge in magnitude beyond the failure point, the previously intact rock will move (Enderlin and Alsleben, in press). Movement of the rock can also be achieved when a preexisting mechanical discontinuity reaches its failure point. Therefore, an understanding of the magnitude and orientation of present-day stresses, the magnitude of nearby pressure sources and the spatial orientation of mechanical discontinuities is essential for anticipating reactivation, particularly when hydraulic fracture stimulation is planned where mechanical discontinuities are present. High-pressure fracture fluids can potentially enter the discontinuity, alter the effective stress, and cause mechanical discontinuities to reactivate in shear. When the magnitude of pressure from sources such as pore pressure, drilling fluids, completion fluids, and injection fluids exceeds the reactivation pressure for a particular
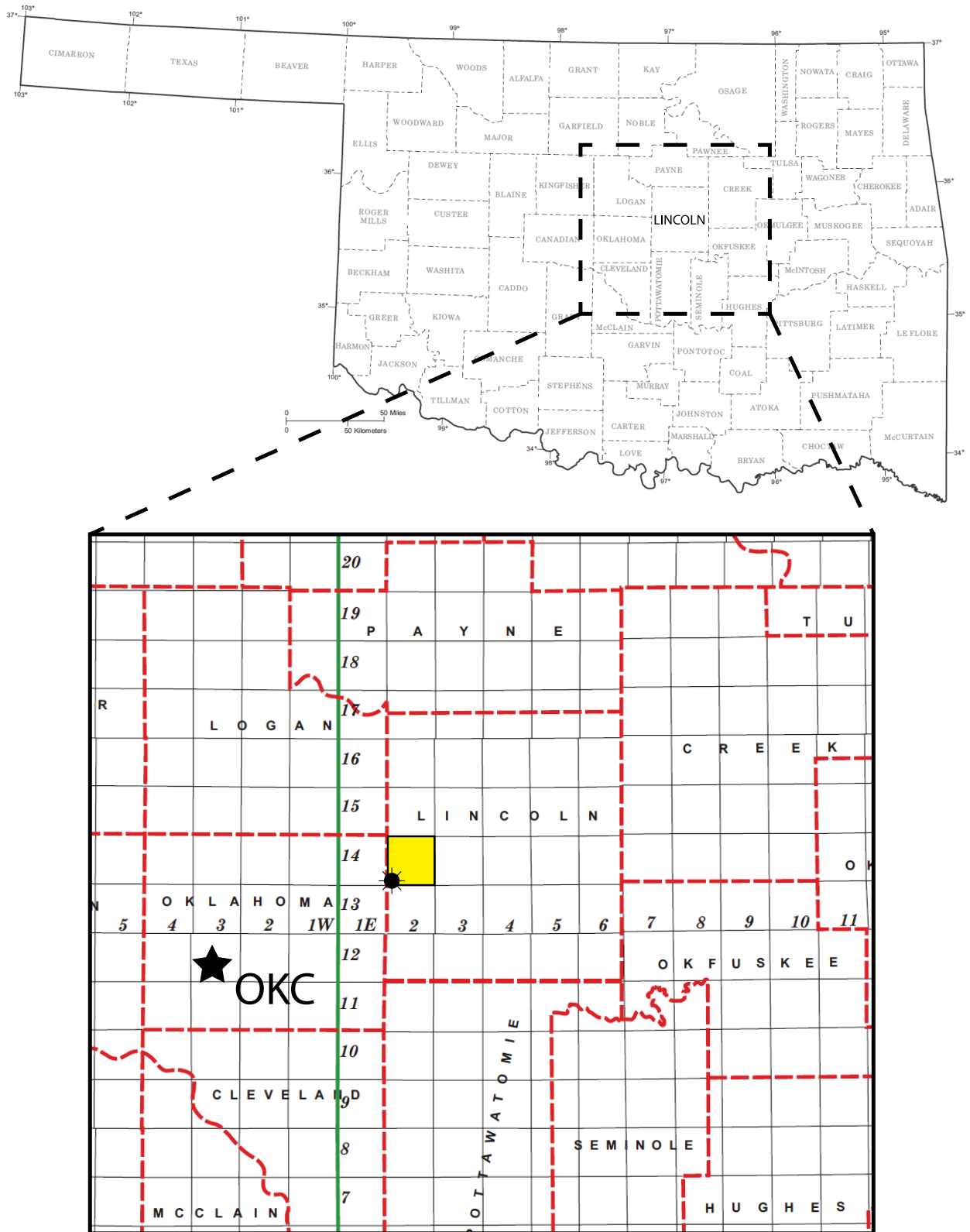
Figure 1: Map of the study area showing townships, ranges and counties in the state of Oklahoma, USA. The whole core data used in this study was collected from the EOG Smith, B. 31 #3 SWD well, located in section 31 of township 14N range 2E, Lincoln County, OK. The star represents the location of Oklahoma City, OK (modified from OGS, 2008).

mechanical discontinuity, then fractures in certain orientations are prone to reactivate and allow fluids to flow along their surfaces. The outcome can be an unwanted diversion of fluid away from the intended target (Enderlin and Alsleben, in press). Using strength data from the core measurements and well logs in conjunction with in-situ stress information derived from well logs and mapped active features, this study evaluates the potential for fluid flow along mechanical discontinuities in the Woodford Shale in Central Oklahoma in the following sections.

GEOLOGICAL BACKGROUND AND PREVIOUS WORK

Depositional History and Environment

The Cherokee Platform extends south from southeastern Kansas and southwestern Missouri into central Oklahoma. The platform is separated from the Anadarko Shelf to the west by the north-south trending Nemaha Ridge (also referred to as the Nemaha Trend) (Figure 2). At its southern terminus near Oklahoma City, OK, the Nemaha Trend serves as the backbone of a structural high surrounded by four deep, petroleum producing sedimentary basins: the Anadarko, Marietta, Ardmore and Arkoma basins. The Woodford Shale and equivalent deposits are found across the Cherokee Platform and Anadarko Shelf and in each basin (Charpentier, 2001).

From Cambrian through middle Mississippian the Arkoma basin and Ouachita fold belt region formed part of a vast stable shelf (the predecessor of the Andarko Shelf/Cherokee Platform) on the southern passive continental margin of North America (Figures 2 and 3). Late Paleozoic subduction of the proto-Atlantic Ocean, which separated North America [Laurentia] and Gondwana, beneath Gondwana initiated the Marathon-Ouachita-Appalachian orogenic event along the paleo-coastline of southeastern North America (Ziegler, 1989). Subsidence of the once stable Arkoma shelf in southeastern Oklahoma began in the middle Mississippian under the load

Figure 2: Map A is a generalized pre-Mesozoic geologic map of the south-central and southeastern part of the USA showing large-scale and selected small-scale tectonic features of the Ouachita orogen, southern Appalachian orogen, adjacent foreland to the north and west, and the Texarkana platform. The McClain County Fault Zone contains the nearest active faults mapped on the surface. Red dot represents approximate location of the EOG Smith B., 31 #3 SWD (modified from Harlton, 1951 and Jusczuk, 2002).

Figure 3: Paleogeographic map of the Late Devonian (360 Mya) showing the collision between the continents of Laurentia (center) and Gondwana (bottom right). The Cherokee Platform formed in central Oklahoma as a stable structural high separating the Anadarko, Arkoma, Ardmore and Marietta basins (modified from Miall and Blakey, 2008).

of thrust sheets advancing from the south, burying the Woodford Shale in the developing

Ouachita Trough (Figure 4 and 5). The trough formed between the preexisting early Atokan shelf

to the northwest and the rising Ouachita Orogen to the southeast (Jusczuk, 2002). Concurrently,

the Anadarko shelf located west of the Cherokee Platform experienced one of its multiple phases

of subsidence. Maximum subsidence rates for the developing Anadarko basin were achieved

during Morrowan and Atokan times, indicating that there was accelerated subsidence during and

immediately following the deposition of the Woodford Shale (Donovan et al., 1983). Similar

subsidence occurred contemporaneously in the Ardmore and Marietta basins in south-central

Oklahoma, isolating the Cherokee Platform and Nemaha Trend as a structural high in central

Oklahoma.

A southward-thickening succession of shallow-water carbonates, which includes the

Arbuckle Group (300 to 2000 m thick) and Viola and Hunton Formations (30 to 600 m thick),

were primarily deposited on the shelf (Byrnes and Lawyer, 1999; Jusczuk, 2002). Thinner, deep-

water black shales and cherts were deposited in the southern part of the developing Arkoma

basin. Carbonate deposition on the shelf was continuous, but during the Middle Ordovician a

cyclic rise and fall in eustatic sea level resulted in four distinct influxes of terrigenous sediment

sourced from the northeast, all of which were deposited to form the Simpson Group (Sutherland,

1989). In the Late Devonian, a disconformity developed on the shelf that was subsequently

overlain by the transgressive Sylamore/Misener Sandstone and the organic-rich Chattanooga-

Woodford Shale. Moving away from the developing Cherokee Platform into the neighboring

basins, both the transgressive surface at the base of the Woodford Shale and the contact with the

overlying silt-rich Sycamore Lime transition from disconformity to angular unconformity

(Figure 5) (Johnson and Cardott, 1992). In addition, sediment derived from multiple sources
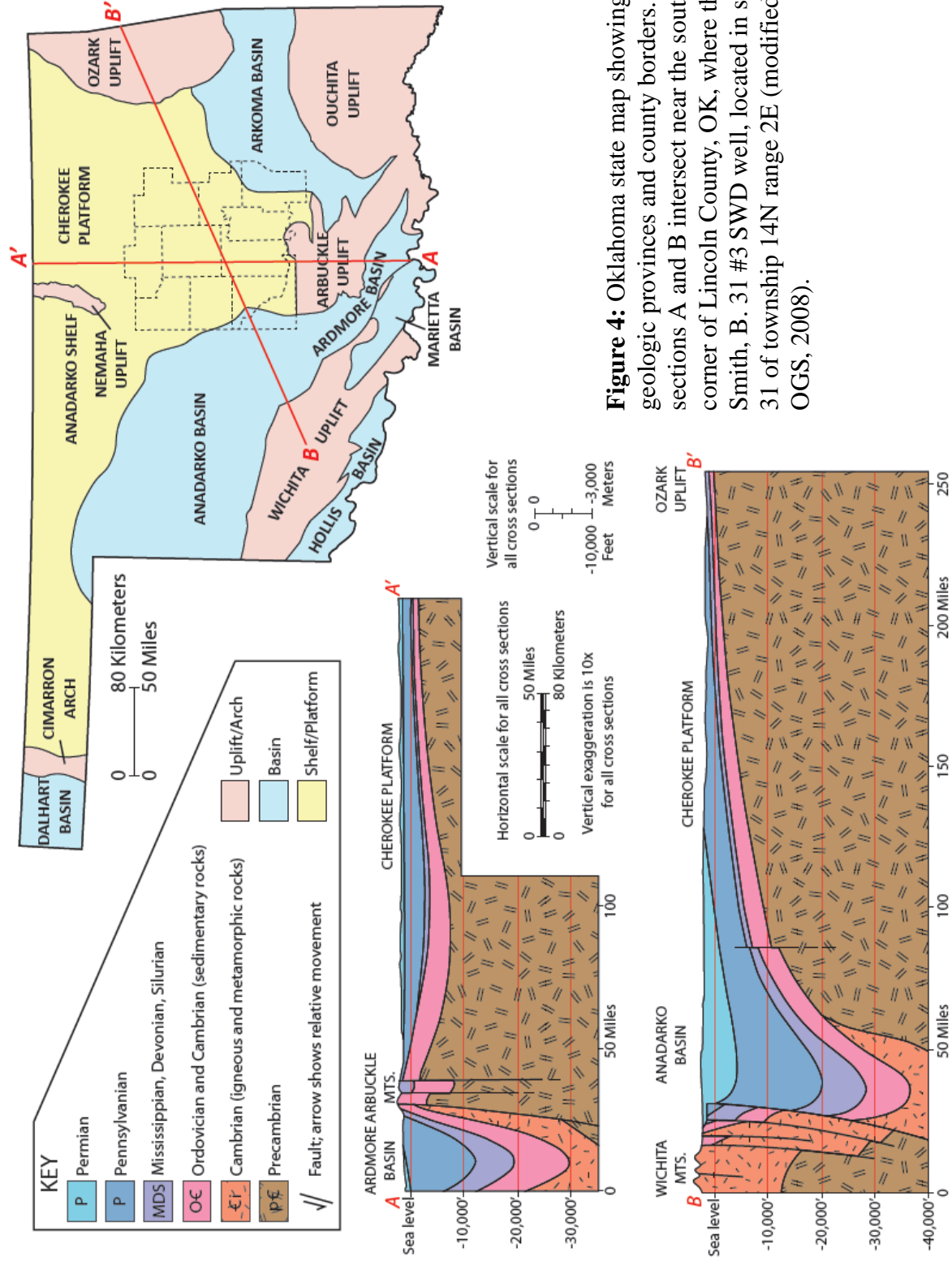
Figure 4: Oklahoma state map showing major geologic provinces and county borders. Cross sections A and B intersect near the southwest corner of Lincoln County, OK, where the EOG Smith, B. 31 #3 SWD well, located in section 31 of township 14N range 2E (modified from OGS, 2008).
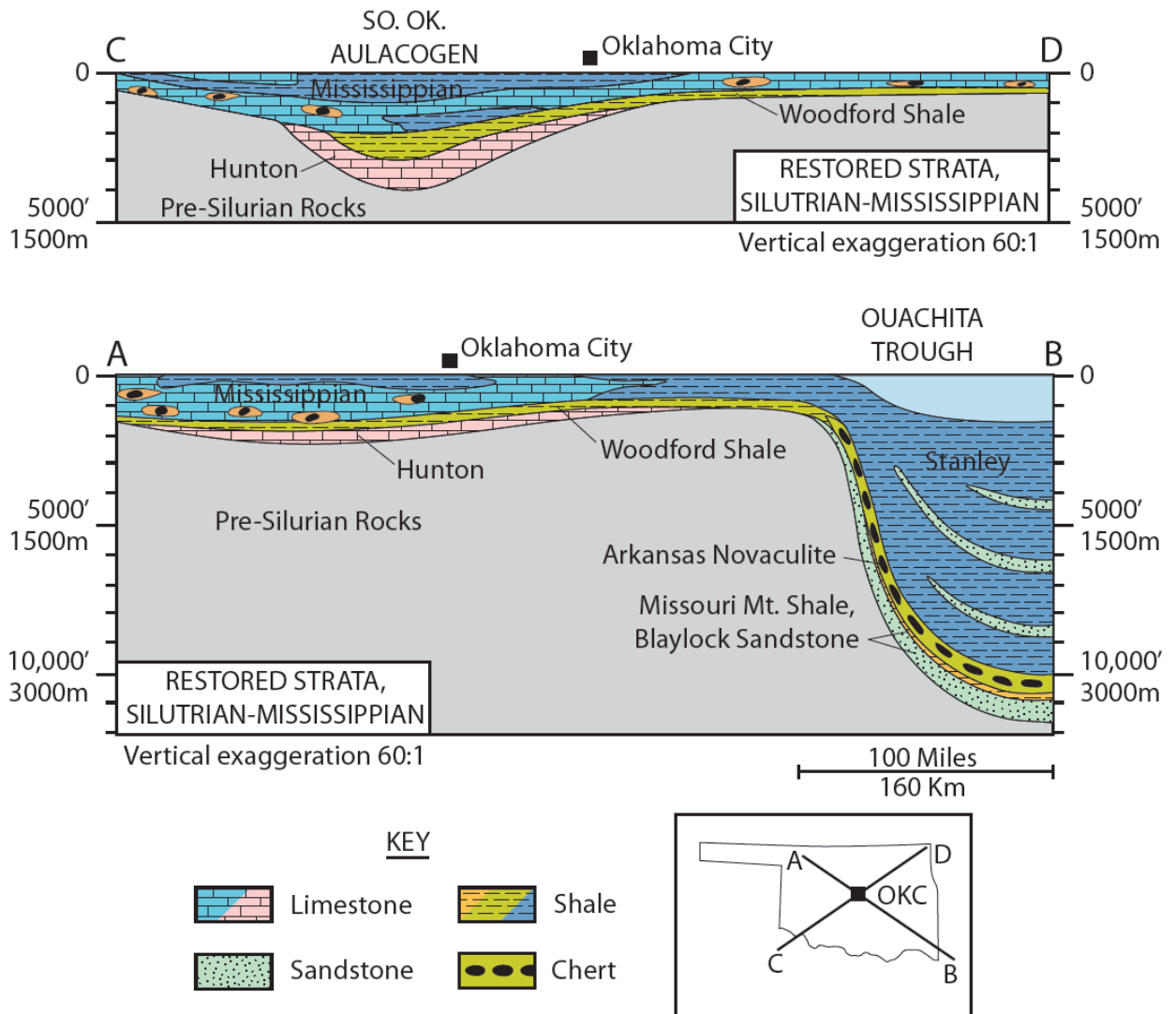
Figure 5: Schematic cross sections showing the restored thickness of strata in Oklahoma from the Silurian to the Mississippian. Note that the Woodford Shale transitions into the Arkansas Novaculite as the depth of deposition increases. Little or no chert is present on the Cherokee Platform, where this study is carried out. Adapted from Johnson and Cardott (1992).

increased the subsidence further. Thick flysch-type deposits of the Stanley and Jackfork Groups sourced from the Ouachita orogenic belt were deposited to the south, while terrigenous sediments sourced primarily from the Illinois basin were deposited on the northern part of the Arkoma shelf margin (Byrnes and Lawyer, 1999; Jusczuk, 2002).

By middle Atokan time, down-to-the-south syndepositional growth faults transformed the southern Arkoma shelf into a foreland basin, which was subsequently filled with deltaic and fluvial deposits (Sutherland, 1989). The Arbuckle orogeny (Pennsylvanian/Permian) produced regional folds, but ensuing erosion from the early Mesozoic to present has resulted in the removal of a significant thickness of stratigraphic section from both the Arkoma basin and the Ouachita fold belt (Byrnes and Lawyer, 1999; Allen, 2000). To the northwest of the uplifting Arbuckle orogen, the Cherokee Platform remained relatively unaltered. The preserved stratigraphic record resulting from this entire sequence of events includes only a thin, early Paleozoic section of carbonates and organic-rich shale overlain by a thick section of interbedded sandstone and shale, all of which have subsequently been extensively faulted (Byrnes and Lawyer, 1999; Jusczuk, 2002).

Structural History of the Nemaha Trend

The Nemaha Trend is a buried uplift that forms a ridge through the heart of central Kansas and Oklahoma (Figure 2). It consists of a system of contractional folds and thrusts and strike-slip structural features (Gay, 2003). A combination of several northwest-verging back thrusts with the predominant southeast-verging thrusts has formed V-shaped "pop-up" blocks in many places along the Nemaha Trend. These blocks were subsequently offset by left-lateral strike-slip faults that were likely active after the thrusting had ended and may possibly be active today (Gay, 2003).

Within the Nemaha Trend, several fault zones were initially interpreted using a wrench-fault model. A subsequent seismic-based reinterpretation led by the Oklahoma Geologic Survey indicates that the Wilzetta fault (Figure 2) experienced two distinct phases of deformation: compressional (reverse faulting) during the Hunton orogeny and transpressional (left-lateral strike-slip and reverse faulting) during the Ouachita and Wichita orogenies (Holland, personal communication, 2012). The McClain County Fault Zone (Figure 2) is another fault to which this seismic-based reinterpretation has been applied. The near verticality of the faults at the terminus of the Nemaha Trend makes them more prone to strike-slip motion within the contemporary stress state, resulting in the current phase of deformation in the region (Gay, 2003; Holland, personal communication, 2012).

Central Oklahoma Stratigraphy

Perry (1995) described the Woodford Shale as primarily Late Devonian, but ranging in age from Middle Devonian to Early Mississippian (Figure 6; Charpentier, 2001). Age-equivalent strata from Oklahoma, Arkansas, Texas and New Mexico include the Chattanooga Shale, Misener Sandstone, Sylamore Sandstone, the middle division of the Arkansas Novaculite, upper part of the Caballos Novaculite, Houy Formation, Percha Shale and the Sly Gap Formation (Comer, 2008). These units form onlapping sediments that were deposited diachronously on top of a major regional unconformity, and in the southern midcontinent these same units are the stratigraphic record of a worldwide Late Devonian marine transgression (Johnson et al., 1985; Comer, 1991). The Woodford Shale is stratigraphically equivalent to several North American Devonian black shales including the Antrim Shale (Michigan basin), Ohio Shale (Appalachian basin), New Albany Shale (Illinois basin), Bakken Shale (Williston basin) and Exshaw Formation (Western Canada basin) (Arbenz, 1989; Johnson et al., 1989; Sutherland, 1989).

Figure 6: Generalized stratigraphic nomenclature for Precambrian through Permian strata in central Oklahoma (modified after Charpentier, 2001).

In the Arkoma basin, Oklahoma, the Woodford is confined between the Sycamore Formation (a siltstone interbedded with limestone) and the dolomitic Hunton Formation, and is often informally subdivided into upper, middle and lower Woodford, based on well log responses (Comer, 2008; Abousleiman et al., 2009; Sierra et al., 2010). The Elemental Capture Spectroscopy log run in the Wyche#1, which is a shallow, cored research well located in Pontotoc County, Oklahoma, reveals the three distinct intervals in the formation (Sierra et al., 2010; Figure 7). The clay content of the Woodford varies by interval with upper Woodford averaging ~ 20% clay, whereas the middle and lower Woodford average ~ 30% clay (Blackford, 2007; Slatt et al., 2010).

Although black shale is the most widespread and characteristic Woodford Shale lithology, chert, siltstone, sandstone, dolostone and light-colored shale are also common (Johnson et al., 1985; Sutherland, 1989; Comer, 2008). The best quality reservoirs in the Woodford are siliceous, dense, brittle, organic-rich, thermally mature and naturally fractured. The combination of these elements results in higher production rates, more extensive fracture penetration, less sand-production and slower fracture closure rates during depletion (Comer, 2008).
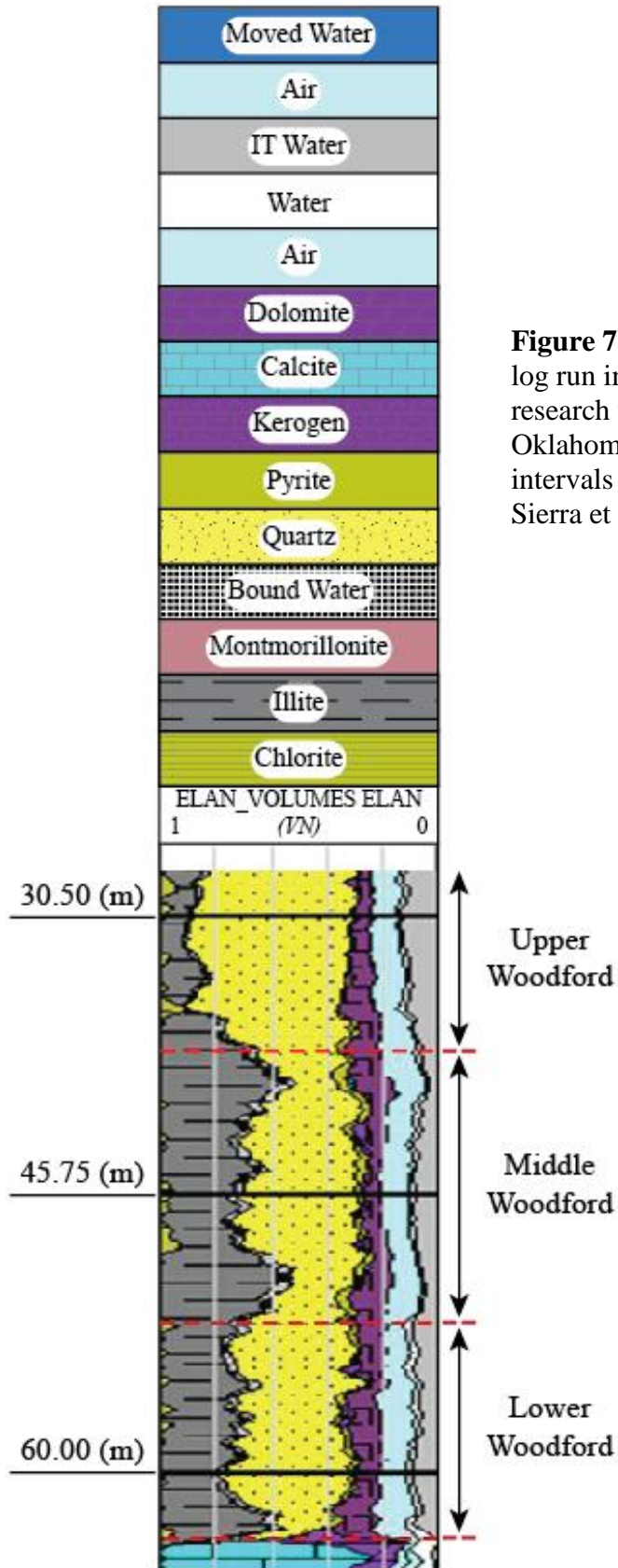
Figure 7: Elemental Capture Spectroscopy log run in the Wyche#1, a shallow, cored research well located in Pontotoc County, Oklahoma. The results reveal three distinct intervals in the formation (modified from Sierra et al., 2010).

Source Rock Properties

Hydrocarbon source rocks, defined as having >0.5 wt% TOC, are attractive targets for unconventional drilling because their hydrocarbons are indigenous and do not depend on the unpredictable and inefficient processes of expulsion from a separate fine-grained source bed, migration through porous and permeable carrier beds, and accumulation in an adequately sealed reservoir (Amsden, 1967; Burruss and Hatch, 1988; Comer, 2008). Source rocks that contain the highest concentrations of organic hydrogen generate the most hydrocarbons. These rocks are typically of lacustrine or marine origin, containing both Type I and Type II kerogen, and they can generate both oil and gas during thermal maturation (Cardott, 1989). Oil-to-rock correlation studies document that the Woodford Shale is a prolific oil source estimated to have sourced as much as 85% of the oil produced in central and southern Oklahoma (e.g., Brenneman and Smith, 1958; Welte et al., 1975; Lewan et al., 1979; Abousleiman et al., 2007; Comer, 2008). The Woodford Shale in the Arkoma basin (Oklahoma and Arkansas) has mean organic carbon concentrations of 4.3 wt% (Comer, 2008). Across the region, the Woodford Shale exhibits a wide range of thermal maturities from marginally immature (Ro = 0.37) to metamorphic (Ro = 4.89) due to dramatic changes in burial depths (Comer, 2008). The mean random vitrinite reflectance of the EOG Smith, B. 31 #3 SWD is 0.55% Ro, based on 30 measurements ranging from 0.47-0.70%. Lower reflectance values (0.42-0.46% Ro) that could be pre-oil bitumen have been excluded due to the similar appearance of bitumen and vitrinite in reflected white light. Large, fluorescent green tasmanites algae are visible in thin section, indicating that the thermal maturity is at the start of the oil window (0.5-0.6% Ro). This observation agrees with the measured vitrinite reflectance value (Figure 8) (Cardott, personal communication, 2012). All of these factors, coupled with the widespread distribution of the Woodford throughout the southern

OPL 1414
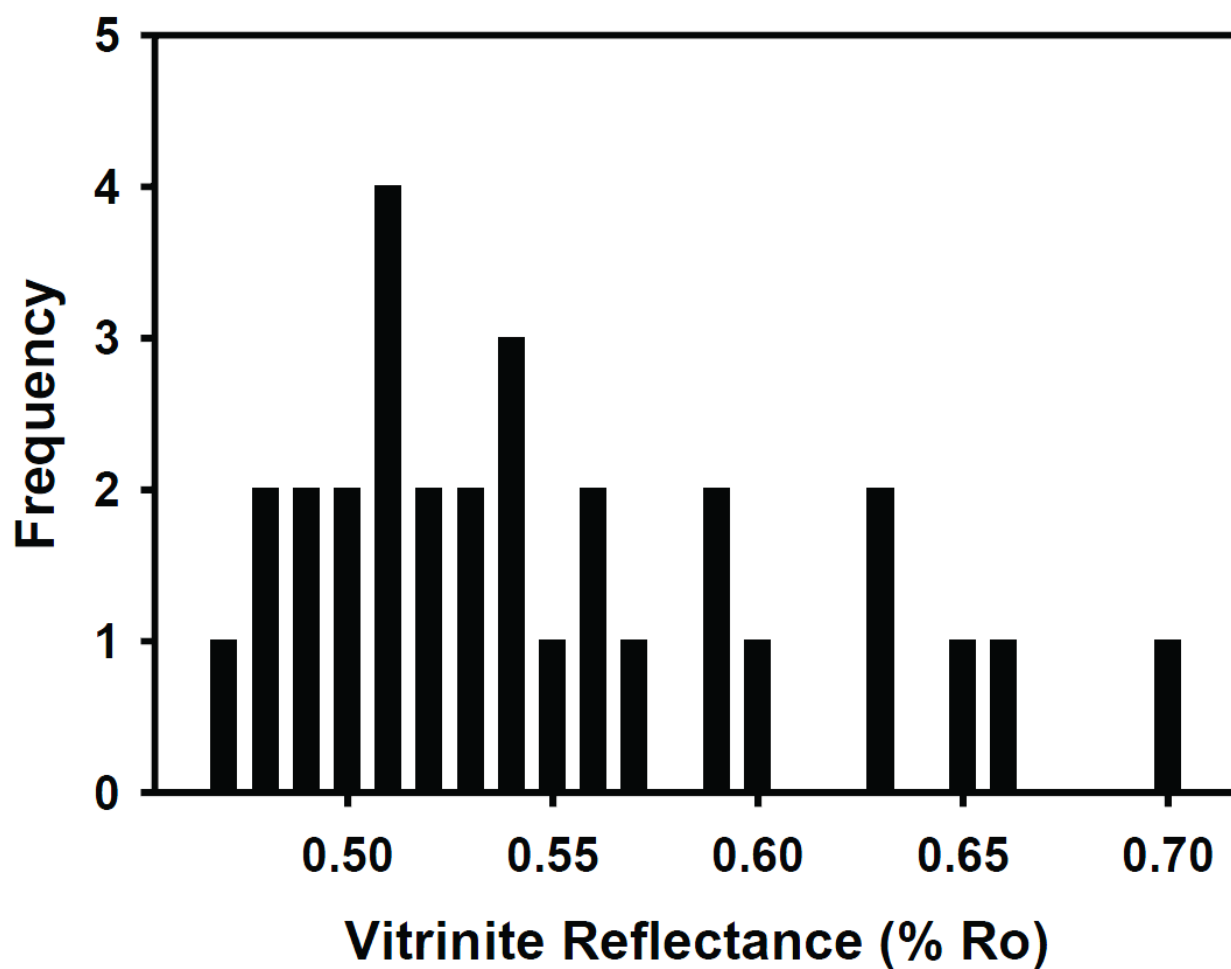
Figure 8: Vitrinite reflectance analysis of the EOG Smith B. #31 3 SWD well (31-14N-2E; Oklahoma Geological Survey Organic Petrography Laboratory sample OPL 1414) (Modified from Cardott, 2012, written communication).

midcontinent of the Midwestern United States, have resulted in large increases in drilling in the formation. Shows visible in cuttings and core and gas responses on mudlogs confirm that the Woodford contains hydrocarbons (Blackford, 2007). From 2003 to 2010, over 1,000 vertical and 300 horizontal wells have been drilled in the Woodford. Of these, 1,200 wells have produced 1.4 million barrels of oil and 560 billion cubic feet (BCF) gas since 2004 (HIS Energy, PI/Dwights, 2009). Publicly announced production rates of up to 10 MMCF per day and estimated reserves of 2.0 to 3.0 BCF per well make it an economically viable target (Sierra et al., 2010). However, its relatively low permeability, estimated to be 45 nD by the pressure pulse decay method, makes hydraulic fracturing essential for production to succeed (Sierra et al., 2010).

General Well Log Characteristics

Well log character throughout the Woodford Shale suggest that the formation has extremely high, natural radioactivity, a non-descript spontaneous potential, high formation resistivity, and low bulk density; the last two log curve responses are caused by the presence of kerogen (Fertl and Chilingarian, 1990). A zone of high, natural radioactivity bracketed stratigraphically between two zones of low radioactivity – the Sycamore Formation and the carbonate-rich Hunton Formation – foremost identifies the Woodford Shale on gamma-ray logs (Comer, 2008; Abousleiman et al., 2009; Figure 9). The lower, middle and upper Woodford have distinct well log signatures whose characteristics can be correlated regionally, providing insights into the rock properties, which in turn give clues regarding the depositional environment of the Woodford Shale. The lower Woodford lies directly atop a Late Devonian regional unconformity (Blackford, 2007; Comer, 2008; Abousleiman et al., 2009). The lower unit has a higher percentage of carbonate, silt and sand and comparatively higher level of natural radioactivity and resistivity with respect to the upper and middle Woodford units (Blackford, 2007; Comer, 2008;
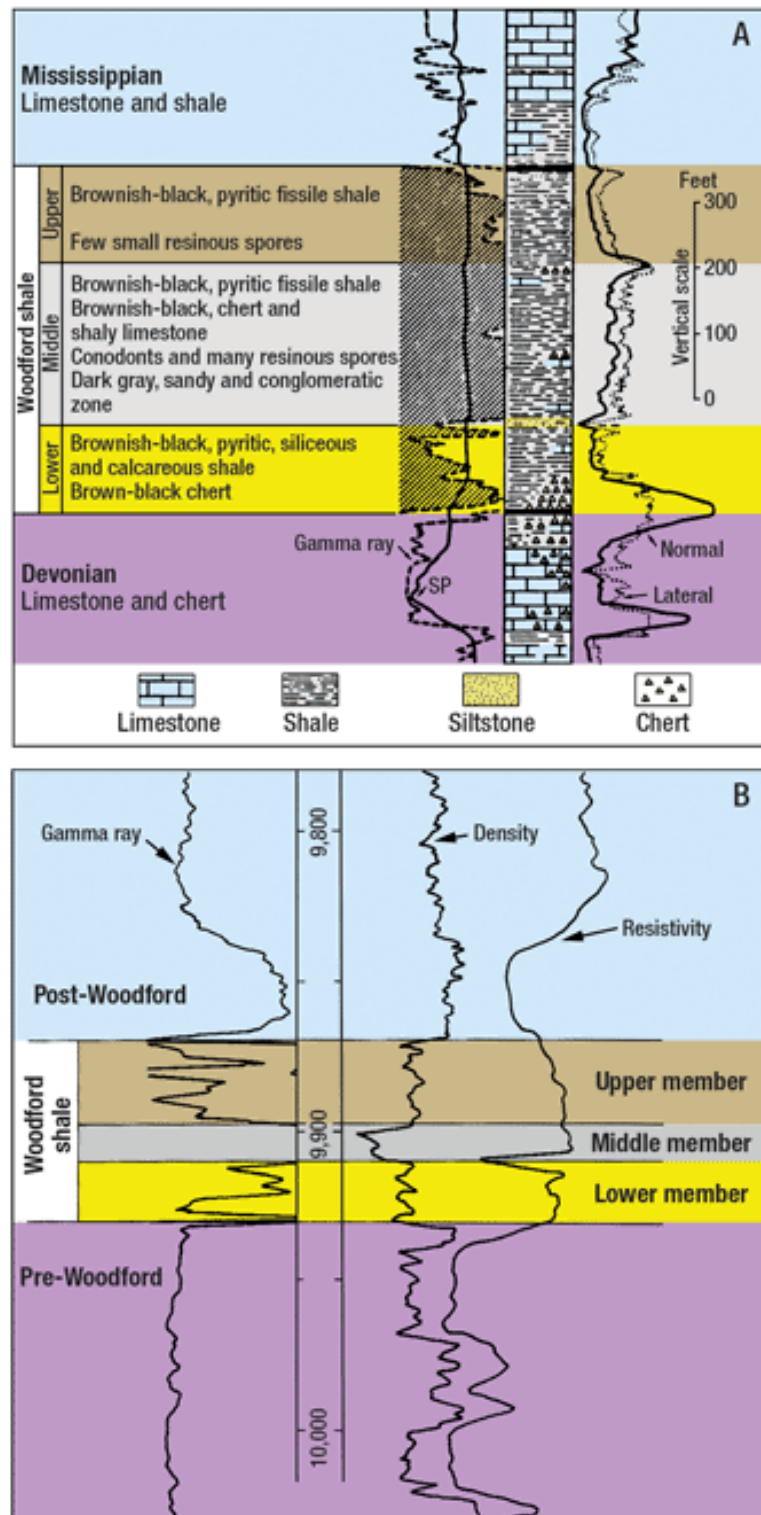
Figure 9: Characteristic well logs over the Woodford Shale interval for the Permian Basin and Anadarko Basin regions. (A) Permian Basin, Winkler County, Texas. (B) Anadarko Basin, Major County, Oklahoma (modified from Comer, 2008).

Abousleiman et al., 2009). These data provide evidence for a shallower marine depositional environment with a greater coastal influence, such as one that would result from a rise in sea level and the development of an unconformity. The middle Woodford unit, which covers the largest mapped area, has the highest radioactivity level, but an intermediate resistivity level, possibly indicating a greater percentage of uranium content in this interval. The middle Woodford consists of a black shale with high concentrations of organic carbon, abundant pyrite, resinous spores and parallel laminae (Blackford, 2007; Comer, 2008; Abousleiman et al., 2009). In addition to low radioactivity, the upper Woodford also has low resistivity values, which possibly correspond with a lower TOC content. The upper unit consists of black shale with few resinous spores and mostly parallel laminae (Blackford, 2007; Comer, 2008; Abousleiman et al., 2009).

APPROACH

Rock Strength Characterization from Core

Rocks can fail under confinement when all stresses acting on the rock are positive, as long as the differential stress (S_1-S_3) exceeds the strength of the material. When rocks are forced to fail under zero confinement, the stress at which failure occurs is called the Unconfined Compressive Strength (UCS), which is commonly measured in pounds per square inch (psi) or Megapascal (MPa) (Figure 10; Enderlin and Alsleben, in press). In this study, UCS values are determined using a handheld point-load penetrometer (referred to as the *Dimpler*) with a calibrated micro-conical point (Ramos et al., 2008; Figure 11). This tool was employed to create indentations or 'dimples', which have been measured to determine the UCS of the rock, on the surface of Woodford Shale core samples. To make a measurement, the tools' conical point is coated in red ink and then impressed at a constant axial load perpendicular to a one square inch size piece of removable tape that is placed atop the surface of interest. The recorded dimples are subsequently catalogued and preserved by placing the tape squares on a flat medium where the dimple is measured with a graduated surface magnifying glass that has a ruler inscribed onto its lens. Geometrical attributes of the dimples (e.g. diameter and depth) created by this tool have been successfully correlated with the UCS (Table 1) and Internal Friction Angle (IFA) values of various rock types for greater accuracy (Ramos et al., 2008). There is a relationship between the IFA and the rate at which the rock gains strength with confinement: for larger IFA's, the rock strength increases faster with increasing confinement. Weingarten and Perkins (1995) used acoustic slowness (μsec/ft) and bulk density (Rho$_b$, g/cm^3), which are commonly found on logs, and correlated between IFA and cohesion (Co), where:

$$UCS = 2\, Co\, \frac{(Sin\ IFA)}{[(Tan\ IFA)(1 - Sin\ IFA)]}$$

(Eq. 1) (Figure 12).
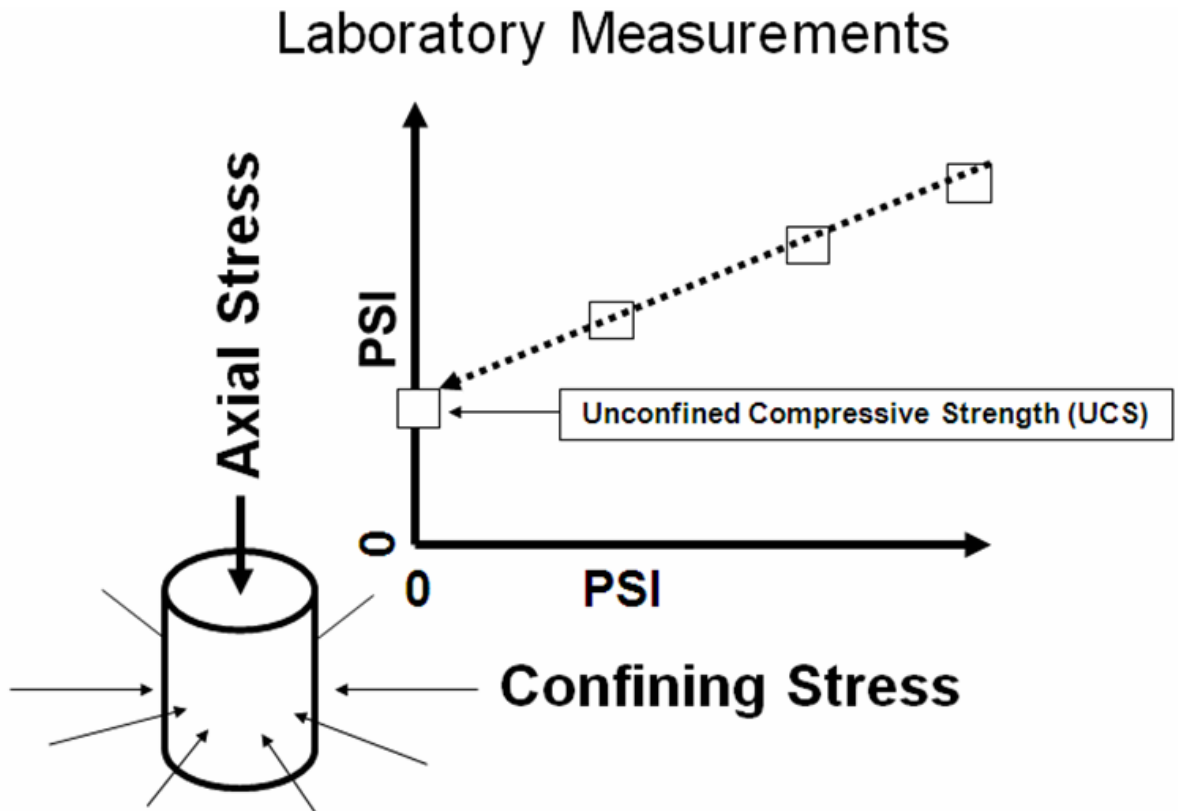
Figure 10: Triaxial compression test geometry and a plot of axial stress at failure for a given confinement from three distinct triaxial tests of companion samples. A best-fit line is projected through the data points and extrapolated to the ordinate (zero confinement), signaling the value referred to as the Unconfined Compressive Strength (UCS). The slope of the best-fit line is related to the rock's Internal Friction Angle (from Enderlin and Alsleben, in press).
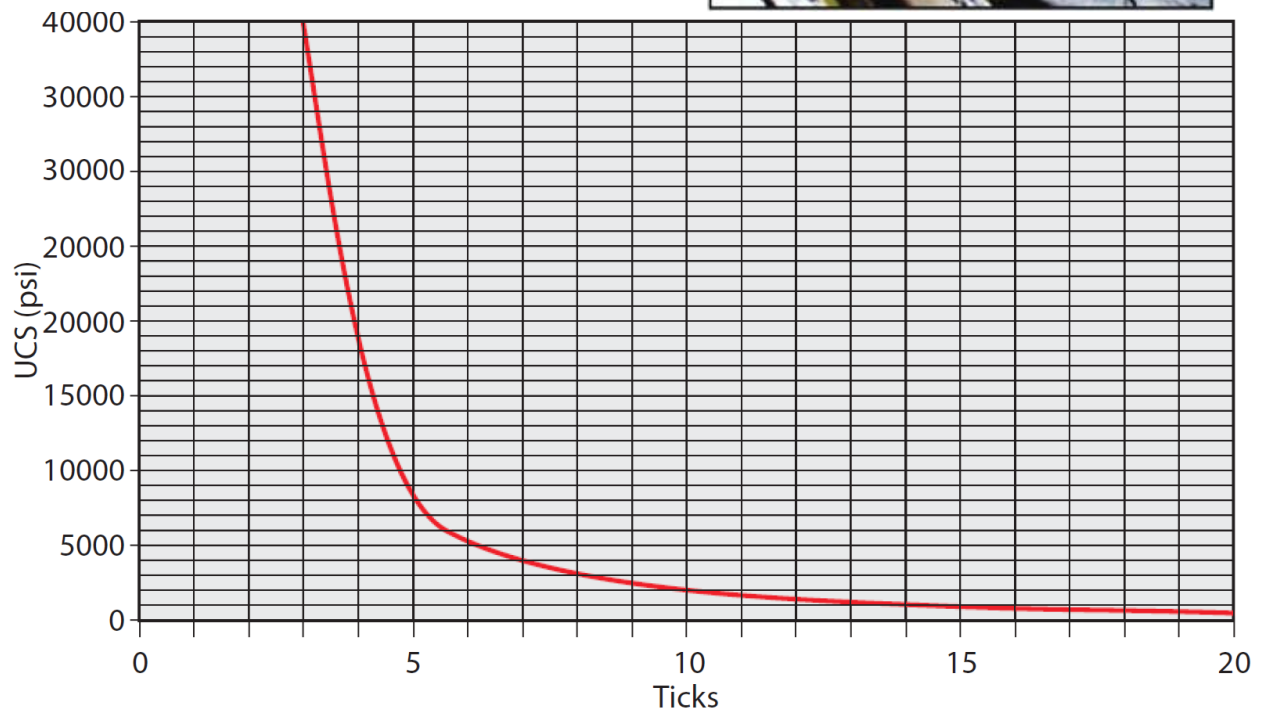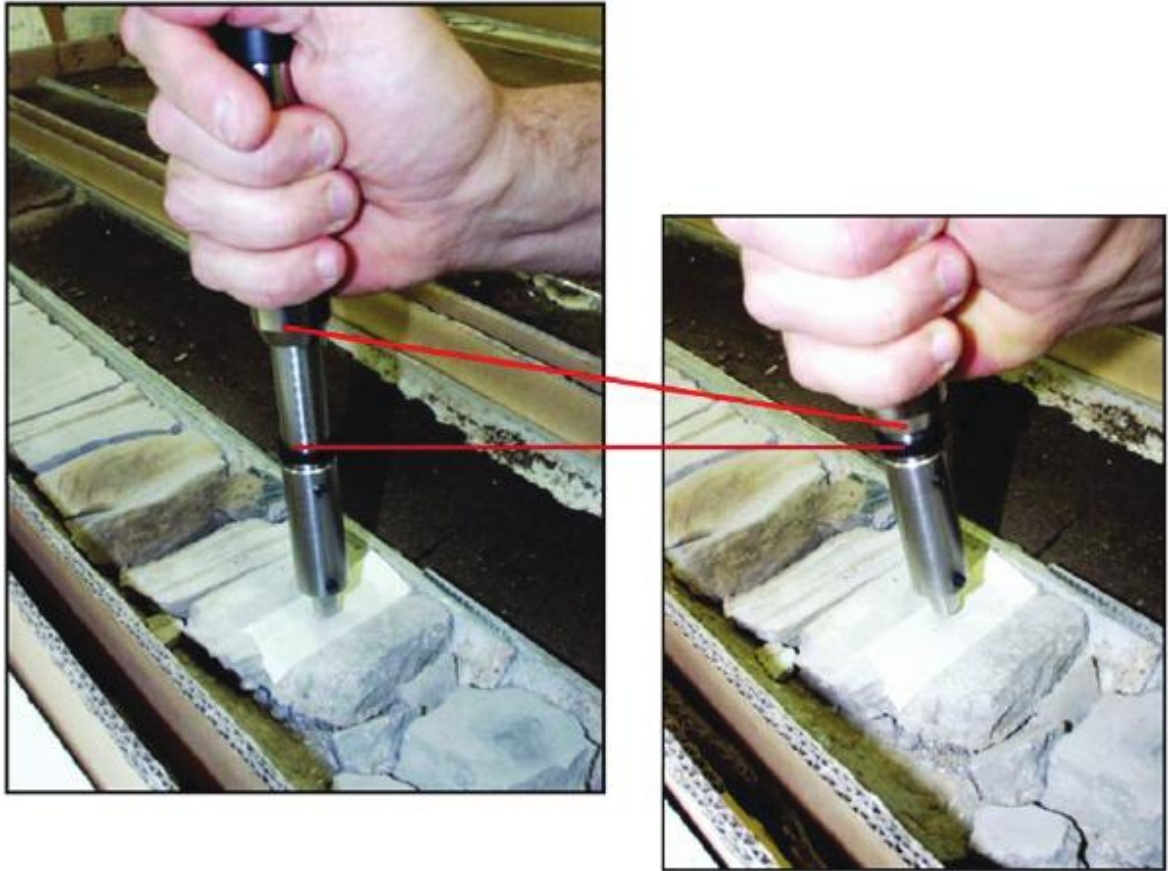
Figure 11: Graphic correlation between the diameter of a dimple created by the micro-indentation tool and the UCS of the sample in psi. Dimple size is measured in "ticks" (each tick = 0.005 inches) (from Enderlin and Alsleben, in press).

Table 1: Reference list of rock formations and associated UCS values (modified from Enderlin and Alsleben, in press).

Rock	UCS in psi, (~ MPa)	Source
Nevada Test Site tuff	1639 (11.3)	Goodman, 1989
Cement (oilfield)	~ 100 (.68) to 6500 (44.8)	Halliburton, 1978
Flaming Gorge shale	5100 (35.2)	Goodman, 1989
Bedford limestone	7400 (51)	Goodman, 1989
Berea sandstone	10700 (73.9)	Goodman, 1989
Micaceous shale	10900 (75.2)	Goodman, 1989
Barnett shale	~ 8000 (55.2) to 11000 (75.8)	Enderlin, 2009, unpublished
Lockport dolomite	13100 (90.3)	Goodman, 1989
James Lime (TX)	~ 7000 (48.3) to 15000 (103.4)	Enderlin, 2009, unpublished
Nevada Test Site granite	20500 (141.4)	Goodman, 1989
Navajo sandstone	31030 (214)	Goodman, 1989
Solnhofen limestone	35500 (244.8)	Goodman, 1989
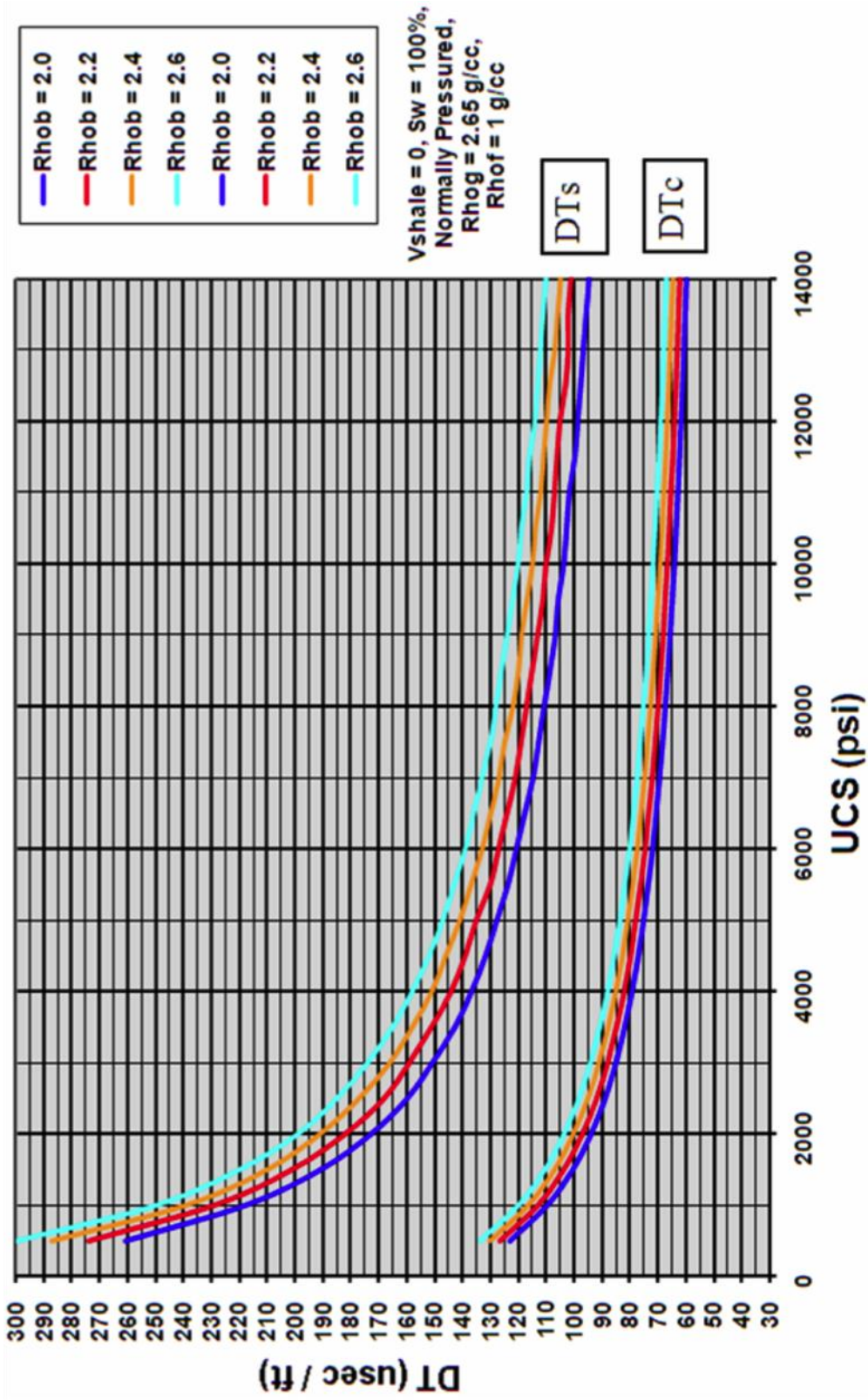
Figure 12: Correlation between bulk density (Rho_b), compressional slowness (DTc), and shear slowness (DTs) with the unconfined compressive strength (UCS in psi) of clean sandstones with matrix density of 2.65 g/cm³ and fully saturated with brine at normal pressure conditions. The formulation presented was developed by Enderlin and Alsleben (in press) using a series of equations that were first presented by Weingarten and Perkins (1995).

The solution by Weingarten and Perkins (1995) makes it possible to cross-reference UCS and IFA values as determined from well logs with the values estimated from nearby core locations using the Dimpler (see Example 1 below). A comparison such as this ensures greater accuracy by providing offset data to the original core measurements and also allows for the interpretation to be extended away from the core location to surrounding wells via log data.

Stress Magnitudes and Directions

Principal (S_1, S_2, S_3) and Component Stresses (S_V, S_H, S_h)

In addition to determining rock strength from core and well logs, constraining the directions of present-day stresses that confine a rock is essential to predicting the mechanical behavior of that rock. A combined stress-strength approach uses image logs, earthquake focal mechanisms, mapped active features and historical stress data to infer stress directions and magnitudes.

Stress and pressure are defined as forces per unit area (e.g., pounds per square inch). U.S. customary units and SI units are widely used and will be given throughout this thesis (pounds per square inch = psi, and megapascals = MPa, where 1MPa = 145.038 psi). Changes in stress and pressure with depth are labeled in psi/foot and pounds per gallon (ppg), where 1 psi/foot is ~ 19.25 ppg. Stress and pressure magnitudes can be plotted on a diagram of stress domains called a 'Stress Polygon' (Figure 13; Moos and Zoback, 1990). In the Stress Polygon, three component stresses – overburden stress (S_V), maximum horizontal stress (S_H) and minimum horizontal stress (S_h) – form a mutually orthogonal system in which two of the stresses reside in the horizontal plane (S_H, S_h) and one in the vertical plane (S_V). "Maximum" and "minimum" refer to the relative magnitudes of the horizontal stresses, where $S_H > S_h$, regardless
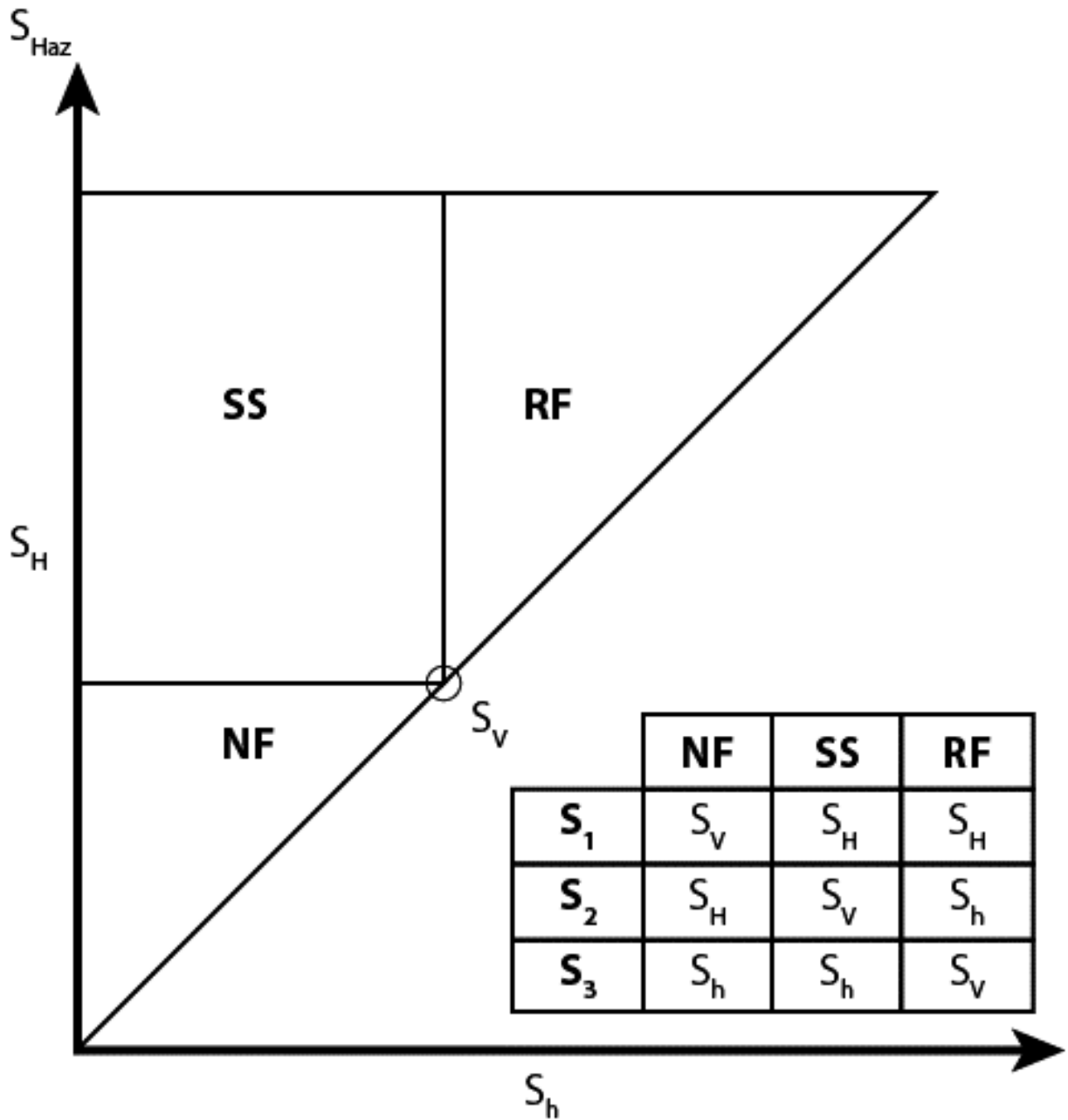
Figure 13: Plot showing the relationship between the three component stresses (S_V, S_H, and S_h) that make up the current stress state (S) and the principal stresses (S_1, S_2, and S_3) within the normal fault (NF), strike-slip fault (SS), and reverse fault (RF) stress domains as defined by Anderson (1951). The magnitude of S_V, which will vary by location, plots along the equality line and constrains the stress domain dimensions (modified from Moos and Zoback, 1990).

of how they each relate in magnitude to S_V. According to Anderson's theory of faulting, the three component stresses S_V, S_H, and S_h are related to the principal stresses S_1, S_2, and S_3 (where $S_1 \geq S_2 \geq S_3$) (Anderson, 1951). While the relationship between the component and principal stresses depends on the fault domain in question, one of the three principal stresses will always be vertical (just like S_V), pointing toward the center of the Earth, while the other two will correspond with S_H and S_h (Figure 13; Enderlin and Alsleben, in press).

Overburden stress (S_V) plays a critical role as a reference for S_H and S_h, and must therefore be described with as much precision as possible. A typical definition for S_V is the stress exerted by the overburden above a specific location in the subsurface. This stress can be expressed mathematically as a function of the measured densities found within that three-dimensional vertical space. The average density value (avRho$_b$, g/cm^3) of the overburden can be determined using the equation

$$\text{avRho}_b = \frac{[\Sigma \text{ of log bulk density (Rho}_b\text{, g/cm}^3)]}{\text{Total \# of Depth Increments Used}}$$

(Eq. 2)

where the log bulk density is the "true density" and the depth derived from logs is equivalent in thickness to the section of rock in question. A hydrostatic pressure of 14.7 psi can support a 33.91 foot tall water column with a density of 1 g/cm^3. Using this premise, an approximate S_V (in psi) can be obtained by multiplying the avRho$_b$ with a constant (0.4335 cc psi/ft g) and the True Vertical Depth (TVD, in feet) (Enderlin and Alsleben, in press). If bulk density data are not available, an estimate of 2.3 g/cm^3 (~ 19 ppg) is a good starting point for most clastic sedimentary rock columns, assuming an average water-filled porosity of about 15% (Zoback, 2007). The elevation of the water table should also be determined and factored into bulk density estimates.

Earthquake Focal Mechanisms and Local Faults

Focal mechanisms (Fig. 14A) are a visual representation of the fault domain derived from the estimated moment tensor, which is a mathematical representation of the movement on a fault during an earthquake. Shaded quadrants show areas of the focal sphere in which the P-wave first motions are away from the source, and white quadrants show areas in which the P-wave first-motions are toward the source. Furthermore, focal mechanisms identify axes of maximum compressional strain (called the "P-axis") and maximum extensional strain (called the "T-axis") resulting from an earthquake.

On Saturday November 5th, 2011, a magnitude 4.7 earthquake ruptured at an approximate depth of 4 km (2.5 miles) in central Oklahoma at 35.553°N, 96.748°W. This event was a foreshock to a magnitude 5.6 earthquake that ruptured the following day at an approximate depth of 5 km (3.1 miles) at 35.537°N, 96.747°W. These two were followed two days later on November 8th, 2011, by a magnitude 4.7 aftershock at an approximate depth of 5 km (3.1 miles) at 35.541°N, 96.754°W (USGS, 2011). By comparison, the EOG Smith, B. 31 #3 SWD is located at 35.65°N, 97.13°W, in Section 31, Township 14N, Range 2E, approximately 22 miles (35km) from the earthquakes, which are found in Section 11, Township 12N, Range 5E (Table 2). Several other magnitude >4.0 earthquakes occurred at nearly the exact same locations during 2010 (Table 2), along with a large number of smaller events. By mapping the location of seismic events across Lincoln County, Holland (personal communication, 2012) demonstrates a clear map trend of a currently unnamed, basement seated fault striking ~ 057° as the source of the earthquakes (Figure 14-A, 14-B). Although the extent of this fault is still being constrained, it is well-recognized and considered by some to be a splay of the Wilzetta fault, which strikes ~ 027° (Joseph, 1987; Gay, 2003). In the southeastern corner of Lincoln County, closest to the study

MW 4.8 Foreshock
November 5, 2011
USGS/SLU Regional
Moment Solution

11/11/05 07:12:45.13

Epicenter: 35.553 -96.748
Mw 4.8

Depth 4km No. of stations: 45

Principal axes:

	Val	Plg	Azm
T	1.92	11	348
N	0.08	66	104
P	-2.00	21	254

NP1: Strike=33 Dip=68 Slip=-172
NP2: 300 83 -23

MW 5.6 Earthquake
November 6, 2011
USGS/SLU Regional
Moment Solution

11/11/06 03:53:10.53

Epicenter: 35.537 -96.747
Mw 5.6

Depth 7km No. of stations: 32

Principal axes:

	Val	Plg	Azm
T	3.40	0	190
N	-0.14	85	95
P	-3.26	5	280

NP1: Strike=55 Dip=87 Slip=-176
NP2: 324 86 -3

MW 5.6 Earthquake
November 6, 2011
USGS WPhase
Moment Solution

11/11/06 03:53:10.00

Epicenter: 35.537 -96.746
Mw 5.6

Depth 11km No. of stations: 41

Principal axes:

	Val	Plg	Azm
T	3.64	2	14
N	0.15	79	118
P	-3.79	10	283

NP1: Strike=60 Dip=81 Slip=-174
NP2: 329 85 -9

MW 4.8 Aftershock
November 8, 2011
USGS/SLU Regional
Moment Solution

11/11/08 02:46:57.04

Epicenter: 35.535 -96.779
Mw 4.8

Depth 6km No. of stations: 57

Principal axes:

	Val	Plg	Azm
T	2.23	10	318
N	-0.29	76	181
P	-1.95	9	50

NP1: Strike=94 Dip=76 Slip= 1
NP2: 4 89 166

Figure 14-A: Synthesis of USGS earthquake summaries for three major events that occurred in 11-12N-5E, about 21 miles southeast of the EOG Smith, B. 31 #3 SWD well from which the core for this thesis was collected. The focal mechanism shows the P-axis (black dot), which represents the axis of maximum compressional strain (modified from USGS, 2011).

30
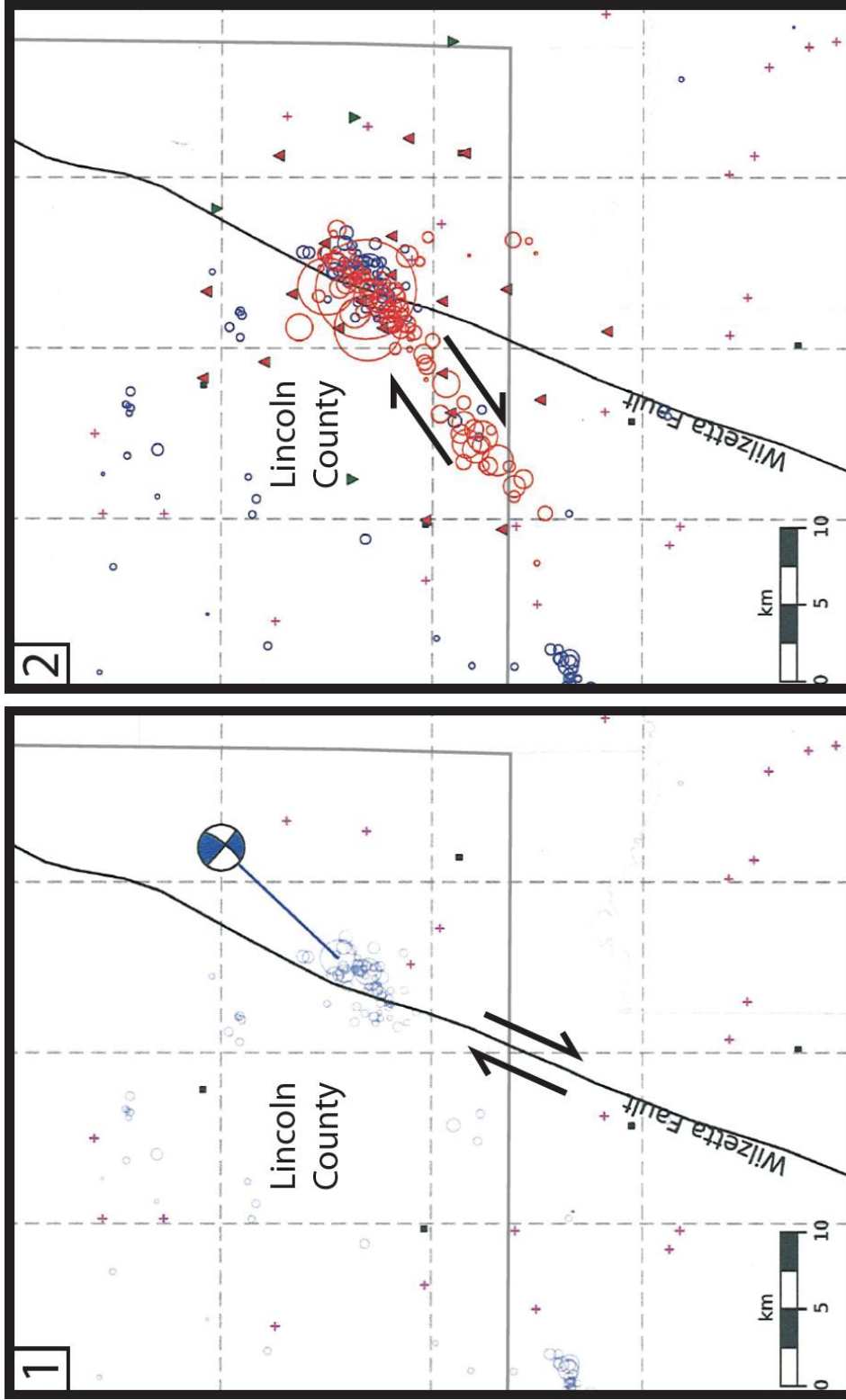
Figure 14-B: Maps displaying the historical seismicity of southwestern Lincoln County, OK from the Oklahoma Geological Survey earthquake database from 1897 to 2009 (shown as red plus symbols). Cities are shown as black squares and the corner of Lincoln County is outlined by a solid grey line. Map A shows earthquakes from January 1, 2010 to November 4, 2011 as blue circles with size relative to magnitude. The focal mechanism displayed is for the February 27, 2010 Mw 4.3 event. Map B shows earthquakes on November 5, 2011 (shown as red circles with size relative to magnitude). Red triangles are seismic stations deployed by Holland et al., 2011, while green triangles are stations deployed by the USGS. These data provide strong evidence for a right-lateral strike-slip fault striking 057° and dipping 80-85° to the east (from Holland et al., 2011).

Table 2: List of magnitude >4.0 earthquakes occurring in Lincoln County since the drilling of the EOG Smith, B. #31-3 SWD (USGS, 2011).

Event	Date	Location (Lat., Long.; PLSS)[c]	Depth
EOG Smith, B. 31 #3 SWD	2-22-2007	35.65°N, 97.13°W; 31 – T14N – R2E	1.87 km (6132 ft TD)
Magnitude 4.0 Earthquake	1-15-2010[a]		5 km (3.1 miles)
Magnitude 4.1 Earthquake	2-27-2010[a]		3 km (1.9 miles)
Magnitude 4.3 Earthquake	10-13-2010[a]	35.537°N, 96.747°W; 11 – T12N – R5E	13 km (8.1 miles)
Magnitude 4.7 Foreshock	11-5-2011[b]		4 km (2.5 miles)
Magnitude 5.6 Earthquake	11-6-2011[b]		5 km (3.1 miles)
Magnitude 4.7 Aftershock	11-8-2011[b]		5 km (3.1 miles)

[a] 2010 events are shown in blue on Figure 14-A, Map 1
[b] 2011 events are shown in red on Figure 14-A, Map 2
[c] Latitude, Longitude and Public Land Survey System

area, the Wilzetta fault dips steeply (~ 75-80°) to the southeast (Bauernfeind, 1982). According

to the focal mechanisms for recent earthquakes in Lincoln County, OK, the unnamed splay dips

even more steeply to the east (~ 81-87°) than the Wilzetta fault (USGS, 2011).

Focal mechanisms from the three largest earthquakes that occurred between November

5th and 8th, 2011, coupled with the strike and dip of mapped active features such as the Wilzetta

fault, confirm that right-lateral strike-slip faulting is ongoing (Figure 14-A, 14-B; USGS, 2011).

The focal mechanism produced for the foreshock recorded on November 5th, 2011 appears to

have ruptured on the Wilzetta fault itself, as its Nodal Plane 1 is more in line with the orientation

of that structure than with the unnamed splay fault (see Figure 14-B, Map 2 for a comparison).

The two subsequent earthquakes (and many other small aftershocks) likely occurred on the

unnamed splay. This distinction is confirmed by considering other earthquake focal mechanisms

recorded in Lincoln County, OK, which have an average strike of ~ 060° and dip of 85° (USGS,

2011). The trend of earthquakes that identify this unnamed fault coincide with the orientation of

Nodal Plane 1 (NP1) of the November 6th earthquake making Nodal Plane 2 (NP2) as the

auxiliary plane (Figure 14-A). The focal mechanism representing a large Mw 4.8 aftershock on

November 8th, 2011 implies that deformation (and displacement) is being transferred from the

Wilzetta fault to neighboring discontinuities during earthquakes.

Building a Stress Polygon

Stress and pressure magnitudes can be plotted on a diagram of stress domains called a

'Stress Polygon' (Figure 13; Moos and Zoback, 1990). The Stress Polygon can be viewed as a

map of three stress domains, where the magnitudes of stress for both S_H and S_h are the same

along the equality line that departs from the origin with a positive slope of 45° and divides the

Stress Polygon into two equal triangles. By definition, all stress and pressure values must plot

above this equality line because S_h cannot be larger than S_H. The magnitude of S_V is plotted as a point on the equality line, from which two other lines will originate to divide the remaining useable space into the three stress domains. As defined by Anderson's classification scheme, the lower left triangle represents a normal faulting regime (NF), depicting a situation where S_V is greater than S_H and S_h ($S_V>S_H>S_h$), implying that $S_1 = S_V$, $S_2 = S_H$, and $S_3 = S_h$ (Anderson, 1951; Moos and Zoback, 1990). The upper right triangle represents a reverse faulting regime (RF), depicting a situation where S_H and S_h are both greater than S_V ($S_H>S_h>S_V$), implying that $S_1 = S_H$, $S_2 = S_h$, and $S_3 = S_V$. The rectangle represents a strike-slip faulting regime (SS), depicting a situation where S_H is larger than S_V which is larger than S_h ($S_H>S_V>S_h$), implying that $S_1 = S_H$, $S_2 = S_V$, and $S_3 = S_h$ (Figure 13). An interactive form of the Stress Polygon built in Microsoft Excel (2008) can be used to integrate the component stresses S_H and S_h with the contemporary regional stress regime, the coefficient of sliding friction (CSF, μ), pore pressure, mud weight, Unconfined Compressive Strength (UCS), Internal Friction Angle (IFA) and cohesion (Enderlin and Alsleben, in press). Modifications were made to a template version of this interactive Stress Polygon using data from the specific circumstances surrounding the EOG Smith B., 31 #3 SWD well in order to determine the fault domain at and around the core location. The importance of each of the components of the Stress Polygon will be illustrated in Example 1 below.

Determining the orientation of S_{Haz}

In this study, information on wellbore breakouts or drilling-induced fractures in the immediate vicinity of the core location were the primary target for determining the stress directions and magnitudes of the contemporary stress field. The orientation of fractures in the subsurface is commonly determined using wellbore imaging logs. Imaging logs produce a picture of the rocks using either resistivity or ultrasonics, and have the capability of imaging

sedimentary rock layers of varying thicknesses, contacts, unconformities, natural and drilling

induced fractures, veins and vugs (Hyne, 2001). Attempts to acquire image logs near the EOG

Smith, B. 31 #3 SWD to view fractures in the Woodford Shale at depth were unsuccessful.

Unfortunately, no natural fractures could be clearly identified in the core itself either.

Published fracture data from the Woodford Shale in proximity to the EOG Smith, B. #31-

3 SWD core location are rare and limited data come from a surface quarry near the town of Ada

in southeast Pontotoc County, OK (Slatt et al., 2010), 70 miles (113 km) to the southeast of the

core location. In an effort to better understand the natural fractures of the Woodford Shale, Slatt

et al. (2010) integrated laser imaging detection and ranging (LIDAR) data, 2D seismic lines, well

logs and core from a shallow well drilled behind the quarry wall. A total of 280 extensional

fractures measured using LIDAR were categorized in two groups: Group 1 is an older,

systematic set with a median strike of $085°$, and Group 2 is a younger, nonsystematic set with a

median strike of $045°$ (Figure 15; Slatt et al., 2010). Both fracture sets are more or less vertical.

Due to the lack of fracture data in the vicinity of the EOG Smith, B. #31-3 SWD core

location, earthquake focal mechanisms, mapped active features and World Stress Map data

(borehole breakouts) have been used to determine the orientation of S_{Haz} and S_h (Table 3). Fault-

plane solutions from recent earthquakes in Lincoln County, OK (Figure 14-A and B) record

deformation, not stress. These solutions contain two nodal planes, which divide the hemisphere

used for projection purposes into compressional and dilatational quadrants that are colored

yellow and white, respectively. The P- and T-axes are the bisectors of the two nodal planes. They

are not, however, coincident with the orientations of S_H and S_h, but are the maximum shortening
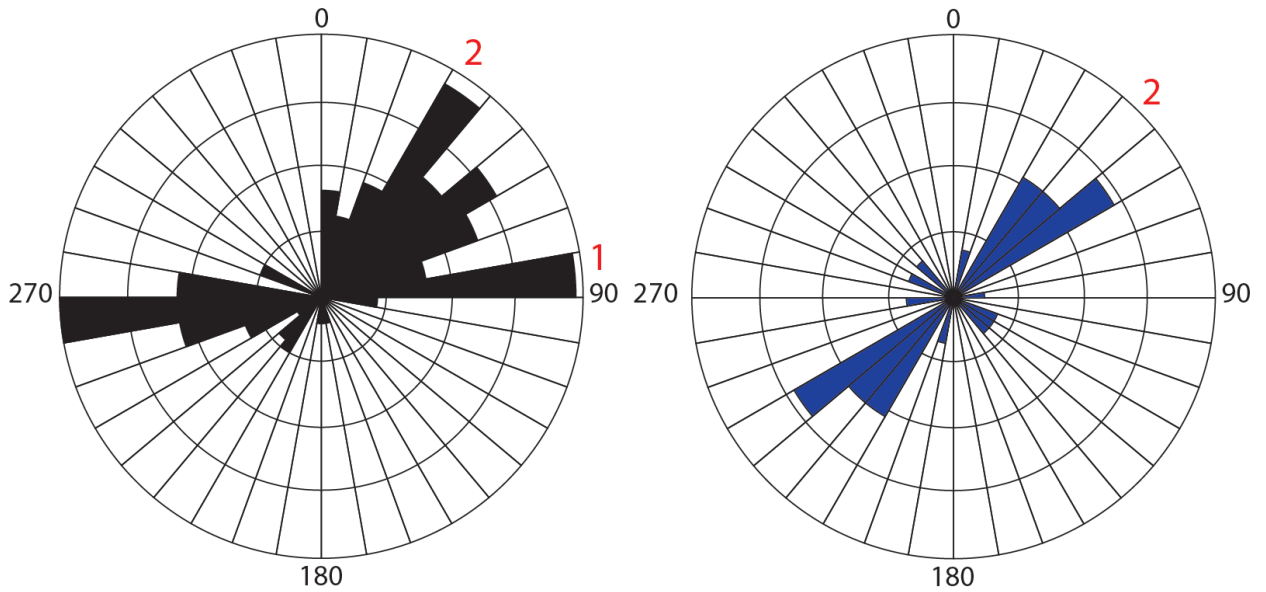
Figure 15: Rose diagrams displaying fracture data from a study performed in the Arbuckle Mountains, approximately 70 miles (113 km) southeast of the EOG Smith, B. #31-3 SWD core location. Fractures were measured using a combination of LIDAR, 2D seismic lines, core and well log data (modified from Slatt et al., 2010).

and maximum extensional strain directions on either of the two nodal planes (Zoback, 2007). It is incorrect to equate the P-axis with S_{Haz}, or even to use the axis to estimate S_{Haz} if the fault plane can be distinguished from the auxiliary plane on the focal mechanism in question. Strike-slip faults are expected to be vertical and strike ~ 30° from the direction of S_H (for μ ~ 0.6) (Zoback, 2007). This point is illustrated by studying the focal mechanism produced by the magnitude 5.6 earthquake that ruptured on November 6, 2011, which depicts a strike-slip fault regime with a P-axis azimuth of 283°. This P-axes is oriented ~ 50° from the strike of the unnamed splay fault striking ~ 057°-237° and nearly perpendicular to the strike of the Wilzetta fault (~ 027°) (Figure 14-B; USGS, 2011). Thus, it is unlikely that the P-axis represents S_{Haz} for this faulting domain. Instead, Anderson's theory of faulting is applied by adding 30° to the strike of the unnamed Wilzetta splay, resulting in S_{Haz} ~ 087°.

Orientation of minimum and maximum horizontal stress may also be determined by observing the orientation of tensile cracks and/or wellbore breakouts on an image log. If either is observed, then S_{Haz} points in the direction of tensile cracks and S_h in the direction of breakouts (Figure 16). Although no tensile cracks were identified in the study area, the World Stress Map (WSM) database shows 18 breakouts oriented an average of ~ 077°. By convention the WSM data orientations show the direction maximum horizontal compressive stress, therefore these data indicate that S_{Haz} ~ 077°) (Figures 16 and 17; Table 3; Heidbach et al., 2008). The higher-than-average coefficient of sliding friction used in this study area (μ ~ 0.62) allows for the angle between S_{Haz} and the expected conjugate fracture pair to form at less than 30°.

The Stress Polygon can also be used to determine the direction of S_{Haz} from mapped active features (specifically faults). To do this, consider the Stress Polygon in map view (Figure 18), where S_V is vertical and the S_H axis is considered the reference direction. The boundaries on
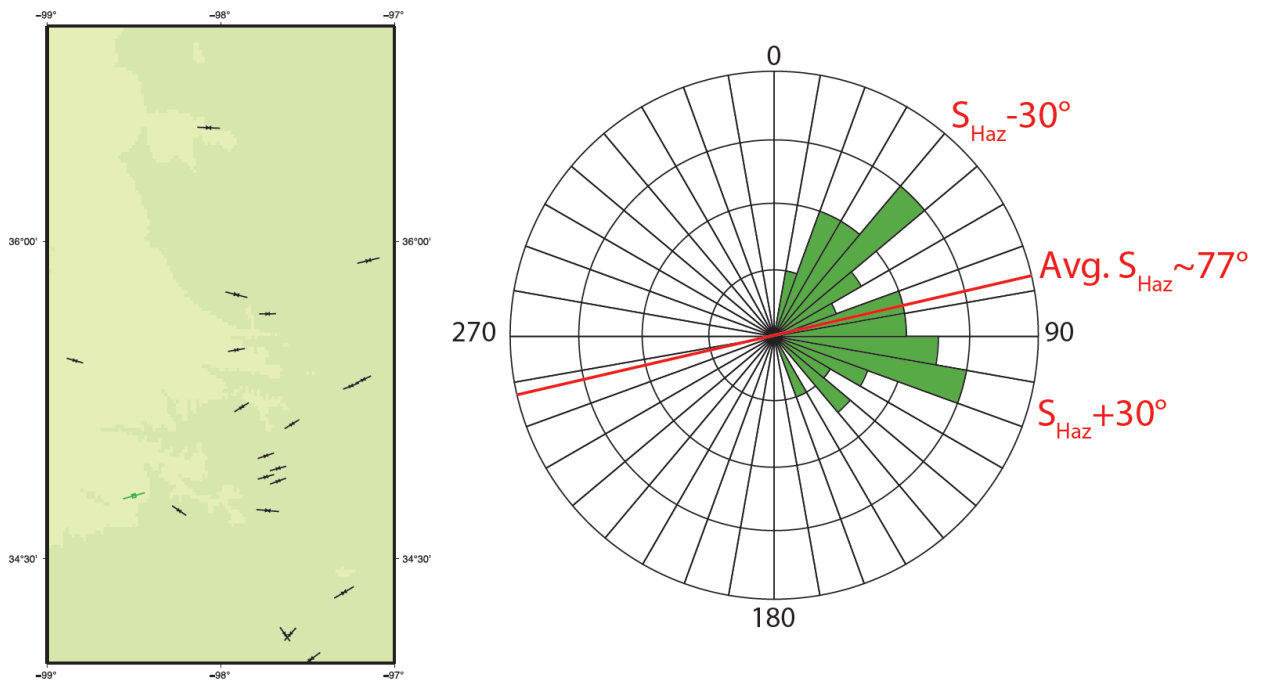
Figure 16: 18 World Stress Map borehole breakout S_{Haz} data points plotted on a rose diagram. Breakout orientations average S_{Haz} ~ 077° (Table 3). 30° was added and subtracted to each of the original S_{Haz} values prior to posting it on the stereonet to illustrate the orientation of fractures most likely to be reactivated within the current stress state if they existed (modified from Heidbach et al., 2008).
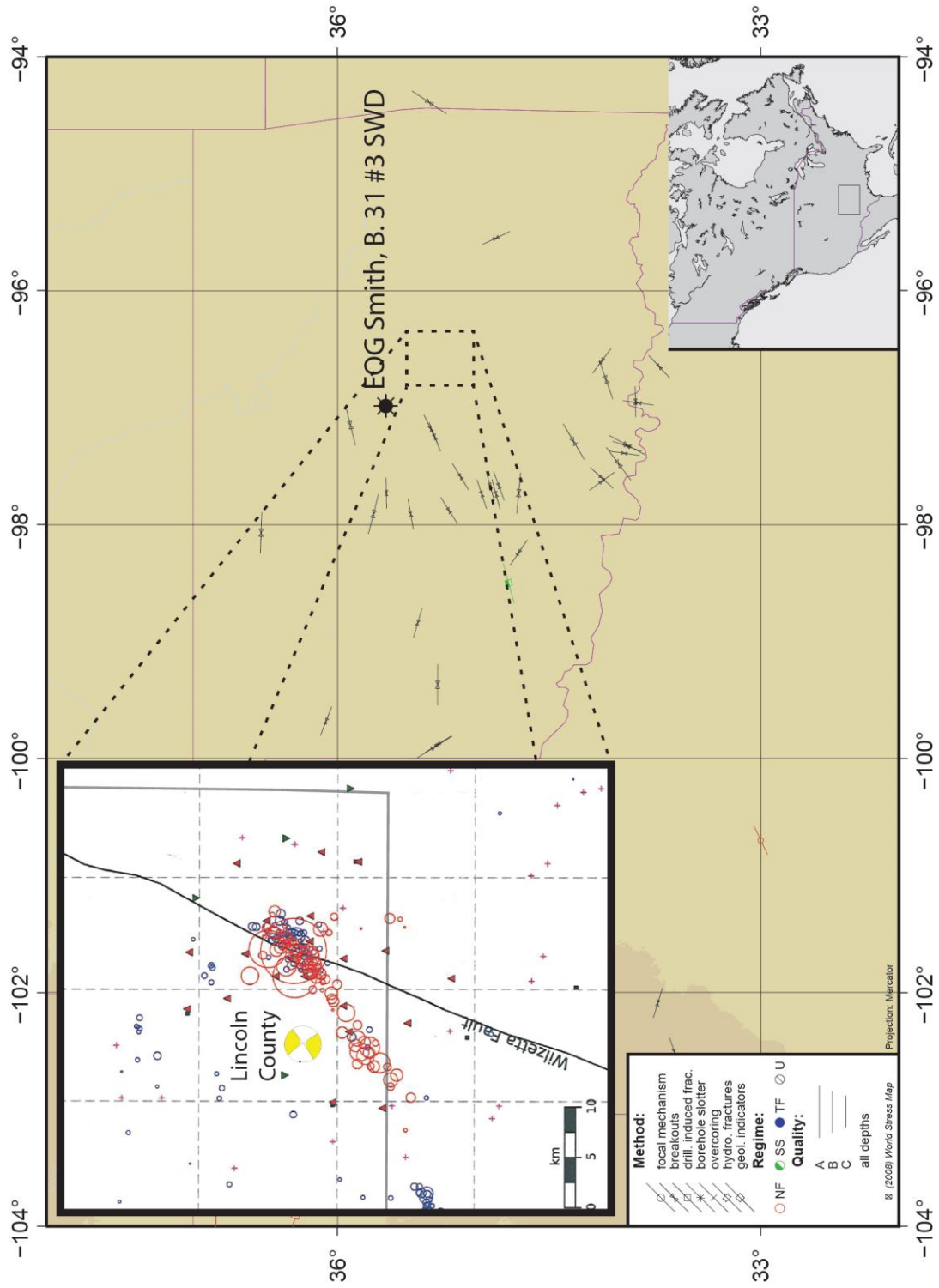
Figure 17: World Stress Map created for the study area. The Oklahoma state border is shown in purple, with its relative location nationwide illustrated in the inset map. Data orientations show the direction maximum horizontal compressive stress. Note that E-W oriented breakouts have been recorded throughout central Oklahoma, indicating that the orientation of S_{Haz} ~077° (see Table 3). The recent earthquake focal mechanisms from central Oklahoma help to confirm this value of S_{Haz} (modified after Heidbach et al., 2008).

Table 3: Borehole breakout data from the World Stress Map database. Data is displayed on a small inset map and plotted on a stereonet in Figure 16 and on a larger map covering the state of Oklahoma in Figure 17 (modified from Heidbach et al., 2008).

Latitude	Longitude	SHaz	Type[a]	Quality[b]	Regime[c]	Depth	SHaz + 30°	SHaz - 30°
34.73	-97.73	095°	BO	B	U	1.95	125°	065°
34.73	-98.24	124°	BO	C	U	1.88	154°	094°
35.66	-97.73	089°	BO	C	U	2.18	119°	059°
34.02	-97.48	053°	BO	B	U	2.30	083°	023°
34.14	-97.60	042°	BO	C	U	2.53	072°	012°
34.89	-97.74	074°	BO	C	U	4.04	104°	044°
34.93	-97.67	074°	BO	C	U	4.06	104°	044°
35.49	-97.91	080°	BO	C	U	3.87	110°	050°
35.14	-97.59	058°	BO	C	U	2.71	088°	028°
35.44	-98.84	106°	BO	C	U	4.77	136°	076°
34.99	-97.74	071°	BO	C	U	4.05	101°	041°
35.22	-97.88	057°	BO	C	U	3.85	087°	027°
34.87	-97.67	069°	BO	C	U	3.66	099°	039°
35.75	-97.91	104°	BO	B	U	2.51	134°	074°
35.91	-97.15	076°	BO	B	U	1.24	106°	046°
34.80	-98.50	074°	GFM	B	SS	0.00	104°	044°
35.35	-97.18	064°	BO	C	U	1.58	094°	034°
35.32	-97.25	068°	BO	C	U	1.70	098°	038°

Average SHaz	77°		Average Fracture Strike	107°	47°

[a] Type of stress determination: Breakout (BO), Geologic Focal Mechanism (GFM)
[b] Data Quality Categories (Ranked from high to low): A, B, C, D; and E where only the location, not the S_H azimuth is valid. Longer lines on the map represent higher quality data.
[c] Tectonic regime: Unknown (U), Strike-Slip (SS)
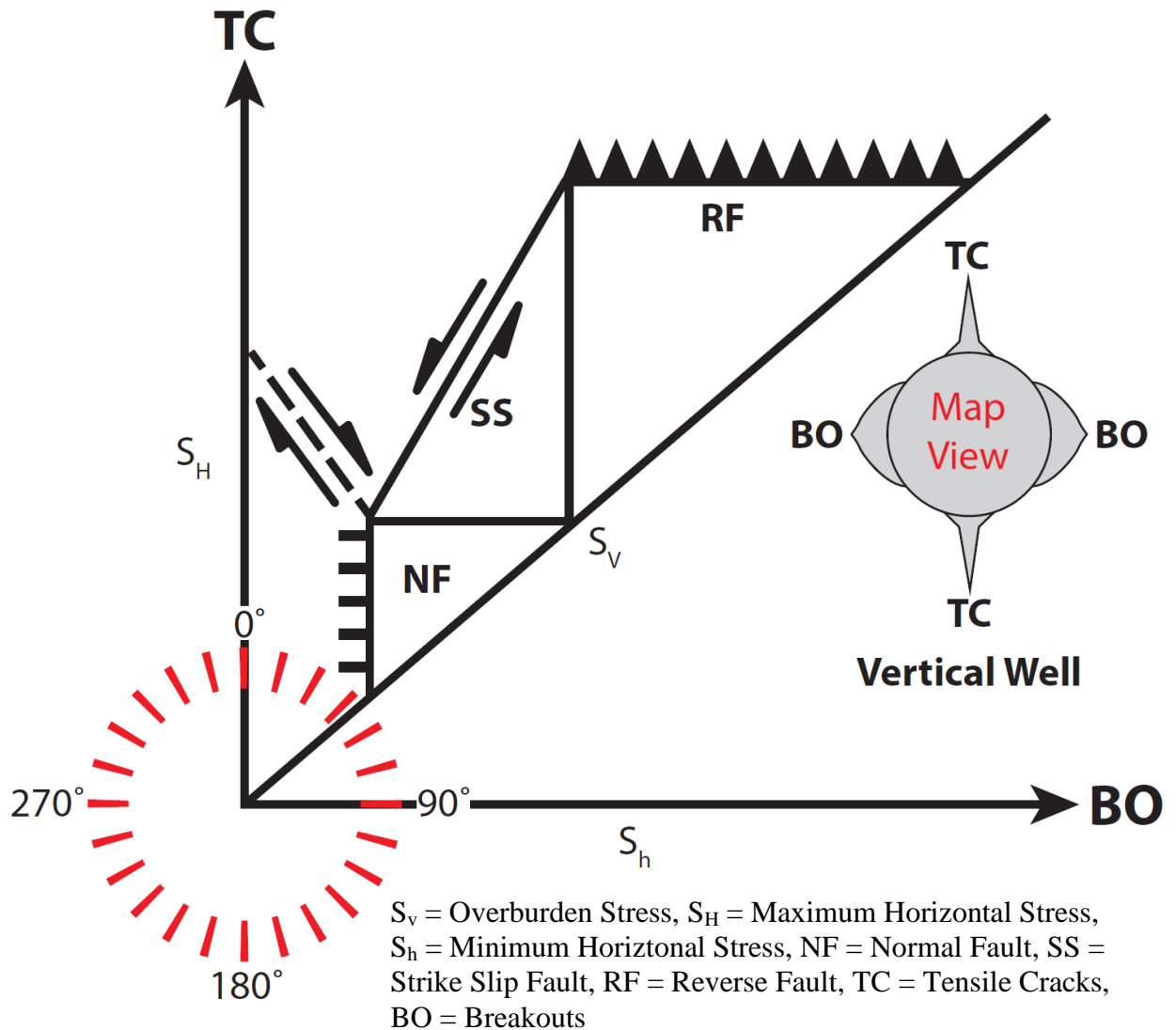
Figure 18: Stress Polygon printed on clear plastic (referred to as the Transparent Stress Polygon), used in conjunction with structural maps and borehole failures (breakouts and tensile cracks) for the determination of S_{Haz}. The borehole in this figure is shown in map view to illustrate the relationship between breakouts and S_h and tensile cracks and S_H (from Enderlin, 2010).

the Stress Polygon (with the exception of the equality line) can be used as the expected strike direction for the associated faults (normal fault = NF, strike-slip fault = SS, and reverse fault = RF). By printing the Stress Polygon on an overhead transparency sheet (referred to as a Transparent Stress Polygon), it can be placed over a structure map showing active faults and be used to determine S_{Haz}. Ensuring that the appropriate polygon strike boundary is aligned parallel to the strike of the mapped faults, the S_H axis is now pointing in the direction of S_{Haz}, and can be read directly with respect to geographic north using the red angular index on the Transparent Stress Polygon (Figure 18; Enderlin and Alsleben, in press). Since the Transparent Stress Polygon is generic, it can be applied to any setting and is used here to determine S_{Haz} on the Cherokee Platform in Central Oklahoma (Example 1). The Wilzetta fault is mapped as a right-lateral strike-slip fault striking ~ 027° (Figure 2; Gay, 2003; Holland, 2011), and by using the Transparent Stress Polygon method the S_{Haz} for the Wilzetta fault is ~ 052°. Although the unnamed splay fault is not yet formally mapped, the trend of the earthquakes corresponds with the strike of NP1 (~ 057°). If we assign NP1 as the fault plane, we can apply the Transparent Stress Polygon method again and determine S_{Haz} for the unnamed splay fault to be ~ 083°. Comparing these two values of S_{Haz} with the estimation of S_{Haz} ~ 077° using borehole breakout data from the World Stress Map, it appears that the unnamed splay is the more likely source of the majority of the earthquakes in this region, not the Wilzetta fault. Therefore, it is expected that earthquakes will continue to occur in groups, with some causing displacement on the Wilzetta fault (as seen by the foreshock focal mechanism in Figure 14-A), the unnamed splay or both.

Taking into consideration the various methods available for determining the orientation of maximum horizontal stress, it is concluded that S_{Haz} ~ 077° for this study area. This value will be tested and applied in Example 1 – EOG Smith, B. #31-3 SWD.

Example 1 - EOG Smith, B. #31-3 SWD

This example is presented to illustrate the methods discussed previously, using strength data gathered from testing core samples with the Dimpler and from well logs in conjunction with in-situ stress information derived from mapped active features (earthquake focal mechanisms, faults and World Stress Map data). The available well log suite for the core location includes the following raster images: gamma ray, lithodensity compensated neutron, array induction (resistivity) and dipole sonic (Appendix 1). These data are integrated into a dynamic Stress Polygon to determine the faulting domain of the region, and thereby constrain the orientation of mechanical discontinuities that are most likely to be reactivated with increasing pressure. The potential for fluid flow along fracture surfaces in the Woodford Shale is dependent upon this combined stress/strength approach.

Whole core extracted from the Woodford Shale at the EOG Smith, B. #31-3 SWD and stored at the Oklahoma Petroleum Information Center (OPIC) in Norman, OK is the focal point of this study. The cored interval extends from a depth of 5198 ft to 5260 ft (1584 m to 1603 m) measured depth (MD), penetrating 61 ft (20 m) of the lower Woodford Shale and one foot (30 cm) of the underlying Hunton Formation. Spectral gamma ray and bulk density logs produced by OPIC in the lab are displayed to scale with a lithologic core description and the dimple measurements (Figure 19). Using the recognizable Woodford Shale/Hunton Formation contact as a marker on which to tie the available well logs, the total thickness of the Woodford Shale at this location is 92 ft (28 m) from 5169 ft to 5261 ft MD (1575-1603.5 m). Indentations created on the surface and along the length of the core using the Dimpler were measured and catalogued at a regular interval. A precise depth, grainsize, Munsell rock-color (for a dry sample), dimple diameter (measured in ticks) and rock strength estimations for each sampling event were
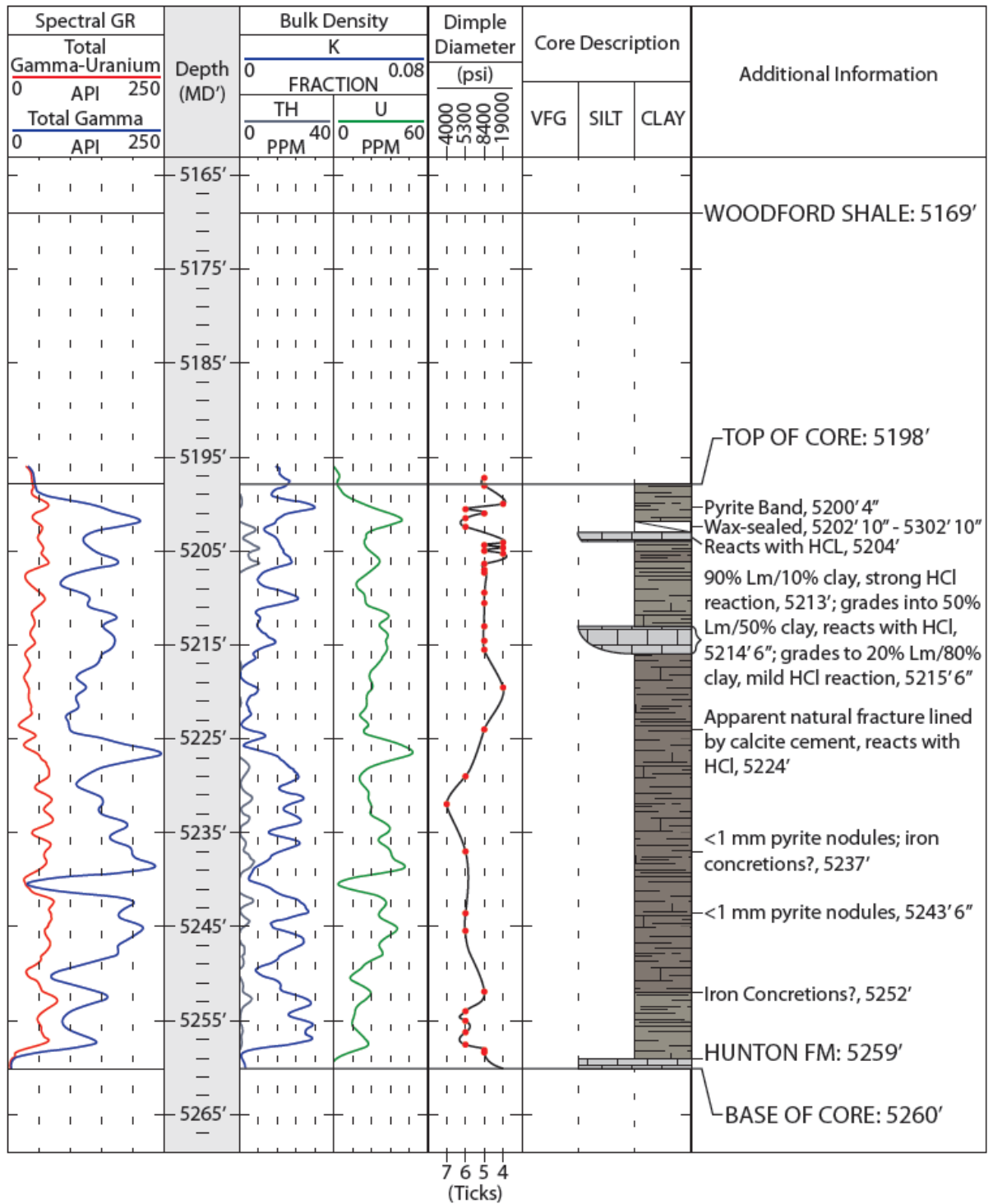
Figure 19: EOG Smith, B. #31-3 SWD core description showing spectral gamma ray and bulk density logs produced by OPIC displayed to scale with the dimple measurements and a lithologic core description. Note the presence of thin pyrite veins and <1mm diameter nodules. Although unlikely to have much effect on the strength of the Woodford Shale at this locale, high concentrations of pyrite and phosphate elsewhere in the Woodford could alter the UCS significantly. Well log curves adapted from written communication with OPIC, 2012.

recorded (Table 4). In addition, whole core photographs were taken (Appendix 2). Care was

taken not to sample portions of the core that were not intact, such as those broken during

retrieval, as values measured therein would not be representative of the subsurface Woodford.

However, natural veins and lithologic changes were sampled as part of an impartial, regular

testing interval. The average dimple diameter of the Woodford Shale at this particular location

on the Cherokee Platform, OK is 5.54 ticks, which corresponds to a UCS of 6100 psi (42.1 MPa)

using the graphical correlation tool presented in Enderlin and Alsleben (in press) (Figure 11). At

a depth of 5216 ft MD (1589 m), the Internal Friction Angle (IFA) and cohesion of the formation

can be determined using the following formulas:

$$IFA = 57.8 - [(1.05)*(Porosity)], \text{ where porosity} = 15\% \text{ (from sonic log)}$$

(Eq. 3)

$$Cohesion = (CCS - UCS)/m, \text{ where UCS} = 6100 \text{ psi (42.1 MPa)}$$

(Eq. 4)

where the Confined Compressive Strength (CCS) is the maximum effective axial stress that a

rock sample can accommodate, and the cohesion is the shear stress necessary to cause failure if

the normal stress is zero (Weingarten and Perkins, 1995).

Table 4: Core description data, including precise depth, grainsize, Munsell rock-color (for a dry sample), dimple diameter (measured in ticks) and the corresponding rock strength (in psi and MPa) for each sampled interval.

Appendix 2 Reference Number	Depth (ft', in")	Grainsize	Munsell Color (Dry)	Descriptive Features (bedding, pyrite, reacts w/ HCl)	Formation	Sample # Trip 1	Sample # Trip 2	Dimple Diameter Trip 1	Dimple Diameter Trip 2	Strength in psi	Strength in Mpa
1	5197' 3"	clay	5Y 4/1		Woodford	1	1		5	8400	58
2	5198' 0"	clay	5Y 4/1		-		2	5	5	8400	58
3	5200' 0"	clay	5Y 4/1		-		3	6	4	19000	131
4	5200' 4"	clay	5Y 4/1	Pyrite Band 2" above	-	2				5300	37
5	5201' 0"	clay	5Y 4/1		-		4		5	8400	58
6	5201' 6"	clay	5Y 4/1		-	3		6		5300	37
7	5202' 3"	clay	5Y 4/1		-		5		6	5300	37
8	5204' 0"	silty clay	5Y 4/1 & N8	reacts with HCl	-		6		4	19000	131
9	5204' 1"	clay	5Y 4/1		-		7		5	8400	58
10	5204' 3"	clay	5Y 4/1		-		8		4	19000	131
11	5204' 10"	clay	5YR 4/1		-	4		5		8400	58
12	5205' 2"	clay	5YR 4/1		-		9		4	19000	131
13	5206' 2"	clay	5YR 4/1		-		10		5	8400	58
14	5207' 0"	clay	5YR 4/1		-	5		5		8400	58
15	5207' 2"	clay	5Y 4/1		-		11		5	8400	58
16	5208' 4"	clay	5Y 4/1		-		12		5	8400	58
17	5210' 5"	clay	5Y 4/1		-		13		5	8400	58
18	5213' 0"	limey clay	N8	90% carbonate material; reacts strongly with HCl	-	6		5		8400	58
19	5214' 6"	limey clay	N8 to 5Y 4/1	50% carbonate material; reacts with HCl	-	7		5		8400	58
20	5215' 6"	limey clay	N8 to 5Y 4/1	20% carbonate material; reacts mildly with HCl	-	8		5		8400	58
21	5219' 6"	clay	5YR 4/1		-	9		4		19000	131
22	5224' 0"	clay	5YR 4/1	Apparent natural fracture lined by calcite cement	-	10		5		8400	58
23	5229' 0"	clay	5YR 4/1		-	11		6		5300	37
24	5232' 0"	clay	5YR 4/1		-	12		7		4000	28
25	5237' 0"	clay	5YR 4/1	<1 mm pyrite nodules; Iron concretions?	-	13		6		5300	37
26	5243' 6"	clay	5YR 4/1	<1 mm pyrite nodules	-	14		6		5300	37
27	5245' 6"	clay	5YR 4/1		-	15		6		5300	37
28	5252' 0"	clay	5YR 4/1	Iron concretions?	-	16		5		8400	58
29	5254' 1"	clay	5Y 4/1		-		14		6	5300	37
30	5255' 0"	clay	5Y 4/1		-		15		6	5300	37
31	5256' 4"	clay	5Y 4/1		-		16		6	5300	37
32	5257' 6"	clay	5Y 4/1		-		17		6	5300	37
33	5258' 4"	clay	5Y 4/1		-		18		5	8400	58
34	5258' 6"	clay	5Y 4/1		Woodford	17		5		8400	58
35	5259' 1"	limestone	N8	reacts with HCl	Hunton		19		5	8400	58
36	5259' 3"	limestone	N8	reacts with HCl	Hunton	18	20	4	5	12500	86
37	5259' 6"	limestone	N8	reacts with HCl	Hunton		21		5	8400	58

The resultant IFA of ~ 42° and cohesion of ~ 160 psi (1.1 MPa) are also integrated in the dynamic Stress Polygon (Figure 20) along with the following preliminary information determined from the available well logs (unless otherwise specified):

a. Depth: approximately 4256 ft TVD (1297 m)

b. Vertical well, less than 2° maximum deviation

c. Pore Pressure: approximately 1990 psi (13.7 MPa) (approximately 0.47 psi/ft)

d. Average Rho_b of Woodford Shale at core location: 2.26 g/cm^3

e. Average Compressional Slowness of Woodford Shale at core location: 88 μsec/ft

f. Average log porosity of Woodford Shale at core location: 15% from logs is adjusted to 10% because high clay content results in exaggerated density porosity values. Given that porosity (ϕ) can be calculated from bulk density (ρb), if fluid density (ρf) and matrix density (ρma) are known using the formula $\phi = (\rho ma - \rho b) / (\rho ma - \rho f)$

g. Static mud weight: 9.7 ppg (2145 psi; 14.8 MPa)

h. Average overburden density approximately 2.35 g/cm^3 (19.6 ppg, 1.02 psi/ft)

Workflow:

1) The initial step requires the determination of the rock strength using well log measurements and the Dimpler.

    a. Rock strength from logs:

        i. Porosity in the Woodford Shale beneath the Central Oklahoma aquifer is expected to contain slightly over-pressured gas, which will alter both Rho_b (2.26 g/cm^3) and DTc (88 μsec/ft) values. By replacing the gas with brine (water saturation, Sw = 100%) and reducing to "normal" pressure, Rho_b = 2.4 g/ccm^3 and DTc = 80 μsec/ft.
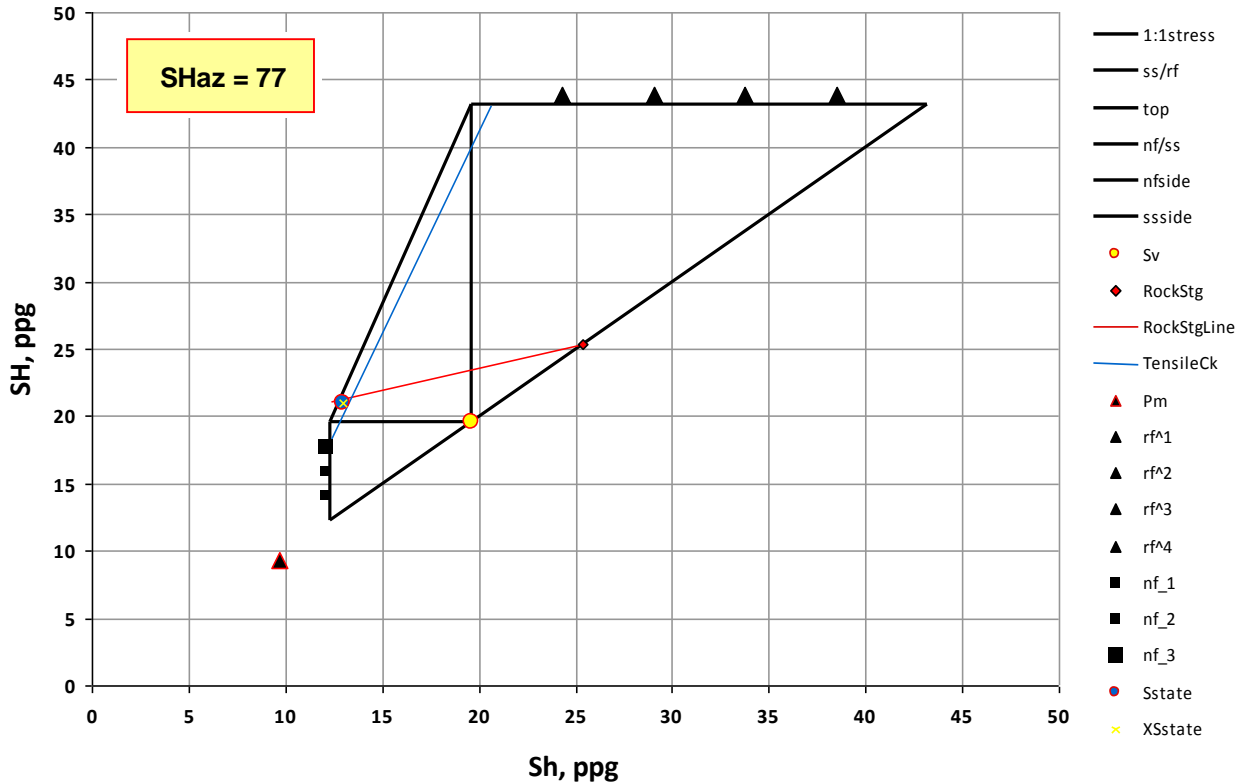
Depth, ft, tvd	Sv	CSF	SH	Sh	Pp	Pm	UCS, ppg	IFA, deg.	Cohesion, psi
	12.3	Fault Marker 0ff = 0			1		Strength Marker 0ff = 0		1
Depth, ft, tvd	**Sv**	**CSF**	**SH**	**Sh**	**Pp**	**Pm**	**UCS, ppg**	**IFA, deg.**	**Cohesion, psi**
4256	19.6	0.62	21	13	9	9.7	27.6	47	204
	4333 psi	0.61	4643 psi	2874 psi	1990 psi	2145 psi	6102	47	1202
			SHaz, deg.	Borehole Stresses		0.7	6102	36.9	204
			77	SH side	Sh side	154.8	1036	47	204
			283	-1 ppg	31 ppg		5	= ppg =	0.9
				-155	6920	ang. to S1 =22	7099 psi	32.1 ppg	= CCS

Figure 20: Interactive Stress Polygon built in Microsoft Excel (2008) as a tool to illustrate the integration of component stresses S_H and S_h with the coefficient of sliding friction (CSF), pore pressure, mud weight, Unconfined Compressive Strength (UCS), Internal Friction Angle (IFA) and cohesion. The effects of modifying the value in any given cell can be clearly seen as the stress polygon changes in shape and size.

      ii. Using Figure 12 (sandstone, Vshale = 0 algorithm), the Unconfined

Compressive Strength (UCS) of the Woodford Shale ~ 5000 psi (34.5 MPa).

For mudstones, however, Vshale = Vclay is between 10-35%, and there

could be up to a ~10% increase over a situation wherein Vshale = 0. After

applying a 10% change to the original UCS estimate, the UCS ~ 5500 psi

(37.9 MPa) (Enderlin and Alsleben, in press).

   b. Rock strength from the Dimpler was determined using the tool methodology as

described in the Approach section above. An average dimple diameter of 5.54

ticks from the core corresponds to a UCS of ~ 6100 psi (42.1 MPa) (Table 4).

2) From the strength data, the Coefficient of Sliding Friction (μ) can be estimated.

   a. Byerlee (1978) suggests a value 0.85, whereas Zoback (2007) suggests using 0.6.

Using UCS of 6100 psi (42.1 MPa) and Figure 21, a μ of 0.62 appears most

reasonable.

3) Stress determination: By applying the information above to a Stress Polygon at 4256 feet

(1297 m) true vertical depth (TVD) (Figure 20), the resulting stress magnitudes are: S_V =

19.6 ppg (4333 psi) (29.9 MPa), S_H = 23 ppg (5085 psi) (35.1 MPa) and S_h = 13 ppg

(2874 psi) (19.8 MPa).

4) Once strength, the coefficient of sliding friction and stress directions and magnitudes are

determined, the reactivation potential can be assessed. Given that S_V = 4333 psi (29.9

MPa), S_H = 5085 psi (35.1 MPa) and S_h = 2874 psi (19.8 MPa), a reactivation map

illustrates the reactivation pressure (P_{fr} in psi) required with any paired strike-dip

combination in order to activate movement on that surface. P_{fr} is calculated using a

coefficient of sliding friction of 0.62 and zero cohesion. Fractures oriented ~ 30° from the
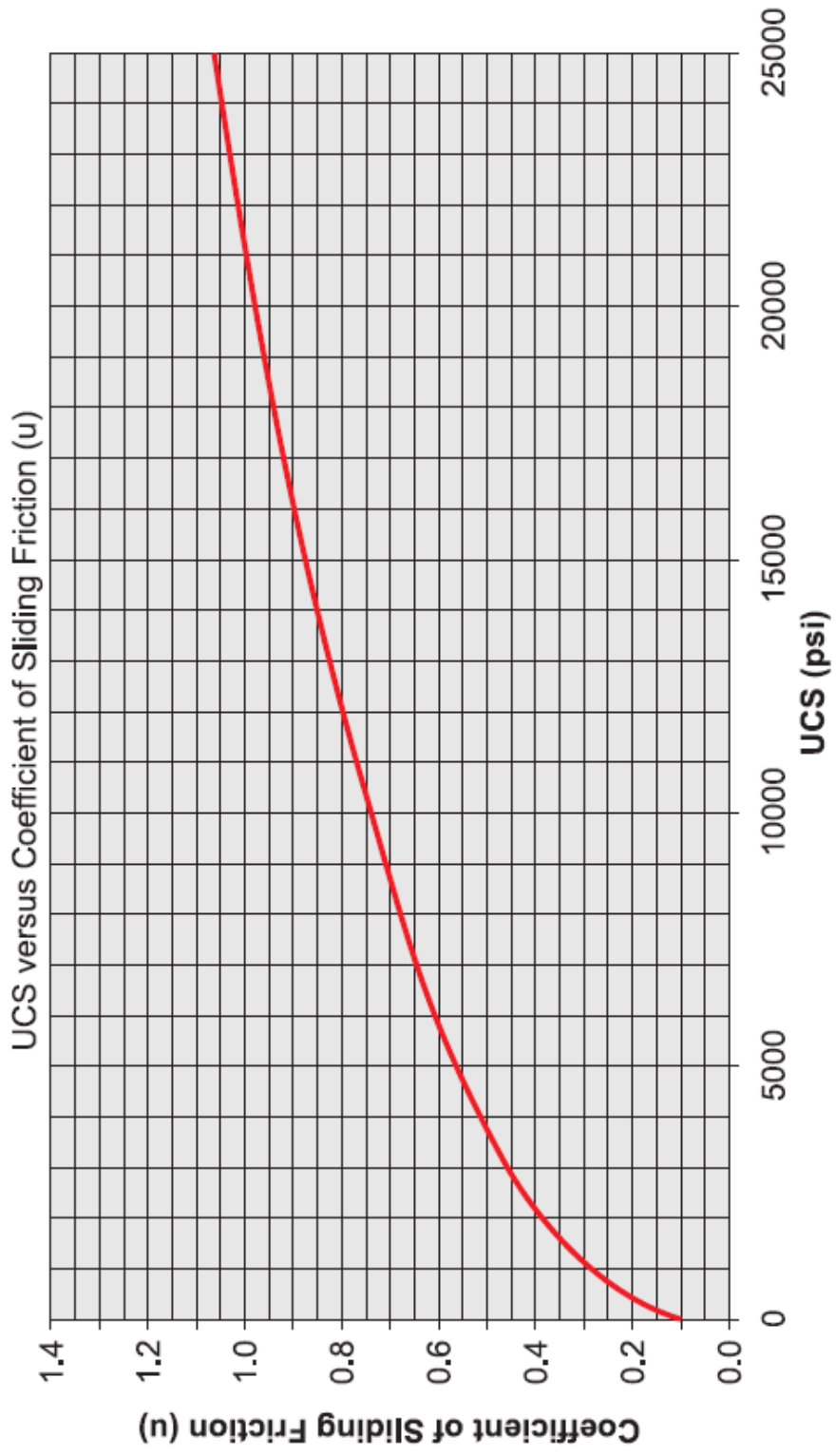
Figure 21: Graphical correlation between UCS and Coefficient of Sliding Friction (μ) (Enderlin and Alsleben, in press).

direction of maximum horizontal stress ($S_{Haz} \sim 077°$) are likely to be reactivated when pressure sources exceed the UCS of the Woodford Shale at or near the EOG Smith, B. #31-3 SWD (Figure 22).

Personal observations and published research both confirm that preexisting mechanical discontinuities (faults and fractures) can be observed throughout the Woodford Shale in Oklahoma, both at the surface and at depth. These structures strike in multiple orientations as a result of a complex deformation history. One such example discussed previously in this study are the fractures comprising Group 2 in the research performed by Slatt et al. (2010) in a Woodford Shale quarry 70 miles (113 km) to the southeast of the EOG Smith, B. #31-3 SWD core location. These fractures form a nonsystematic pattern with a median strike of 045° and near vertical dip (Figure 15) and are younger than Group 1 fractures found in the same quarry. Orientations of the nonsystematic fracture set coincide closely with the expected orientations of one of the fracture sets that would form as part of a conjugate pair of fractures in a region with $S_{Haz} \sim 077°$ as proposed for the study area. Assuming fractures of a similar strike and dip are present in the subsurface around the EOG Smith, B. #31-3 SWD core location, overcoming P_{fr} would result in their reactivation and the movement of fluid along their surfaces. Depending on the purpose of generating fractures, this may be both beneficial or detrimental. In a setting where one is attempting to dispose of fluids via low pressure injection, such as is the case with the EOG Smith, B. #31-3 saltwater disposal well highlighted in this study, the presence of Group 2 fractures is highly desirable. However, if the goal is to create new fractures via high pressure hydraulic fracture stimulation, the presence of a preexisting set of fractures such as Group 2 will likely divert large quantities of fluid from the fracture stimulation and no new mode I opening fractures would be created.
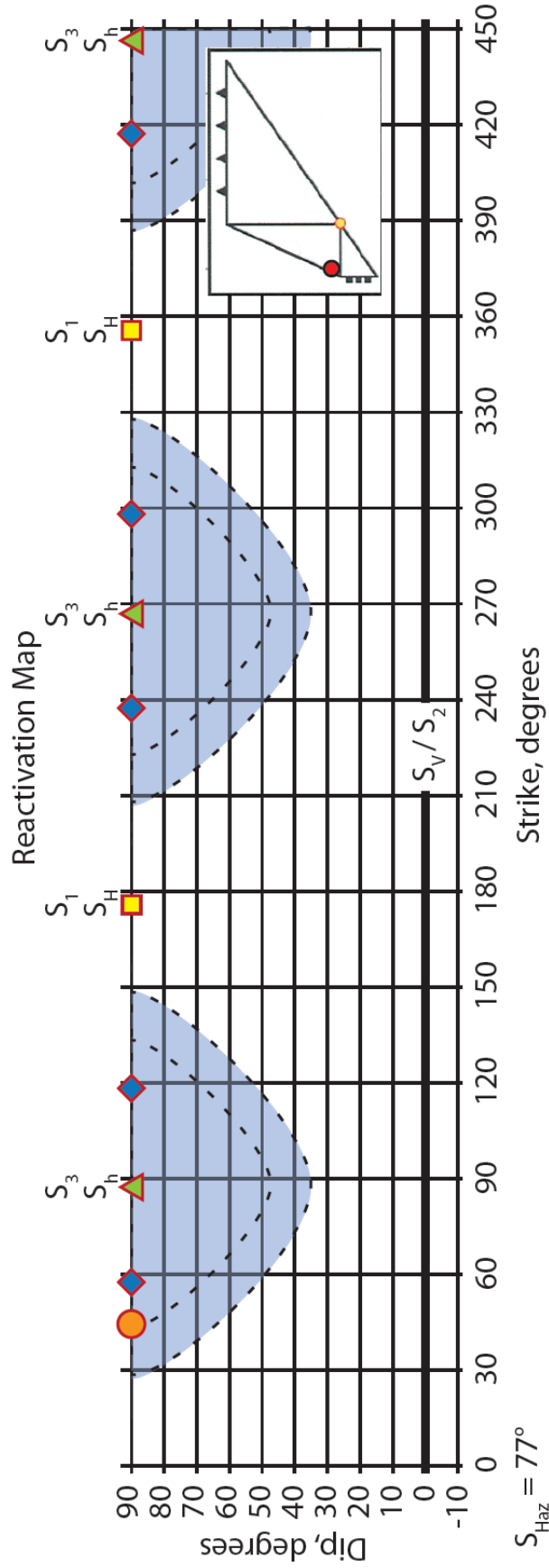
Figure 22: Given that Sv = 4333 psi (29.9 MPa), S$_H$ = 4643 psi (32.0 MPa), and S$_h$ = 2874 psi (19.8 MPa), a reactivation map for the study area illustrates the reactivation pressure (P$_{fr}$ in psi) required with any paired strike-dip combination in order to activate movement on that surface. P$_{fr}$ is calculated using a coefficient of sliding friction of 0.62 and zero cohesion. Vertical fractures oriented ~30° from the direction of maximum horizontal stress (S$_{Haz}$ ~ 077°) can be reactivated if the pressure sources exceed P$_{fr}$ ~ 2000 psi at or near the EOG Smith, B. #31-3 SWD. This pressure, illustrated by the grey shaded region, is sufficient to overcome pore pressure and re-open preexisting mechanical discontinuities with a lower P$_{fr}$, allowing fluid to flow along their surfaces (modified from Enderlin and Alsleben, in press).
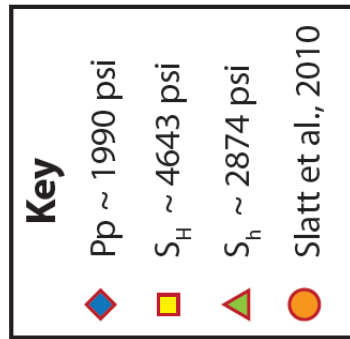
CONCLUSIONS

1. Characterization of the Woodford Shale rock strength from core and well logs collected from the EOG Smith, B. 31 #3 SWD well on the Cherokee Platform, Lincoln County, OK indicates that vertical fractures oriented 30° from S_{Haz} (~ 077°) can be reactivated if the pressure sources exceed a P_{fr} ~ 2000 psi. This pressure is sufficient to overcome pore pressure and re-open preexisting mechanical discontinuities with lower P_{fr}, allowing fluid to flow along their surfaces.

2. Various combinations of strikes and dips with P_{fr} values (in psi) between pore pressure (~1990 psi) and S_h (~ 2874 psi) are likely to be reactivated in the current stress state.

3. The micro-indentation method presented makes it possible to cost-effectively assess the fracture reactivation potential of a formation in both field and laboratory settings.

4. Analysis of the contemporary stress state incorporating earthquake focal mechanisms, mapped active faults and historical data from the World Stress Map provide evidence for an active domain of right-lateral strike-slip faulting in Central Oklahoma.

5. As presented herein, a combined stress/strength approach illustrates the relationship between the reactivation of natural fractures and the hydraulic fracture stimulation of low porosity, low permeability reservoirs.
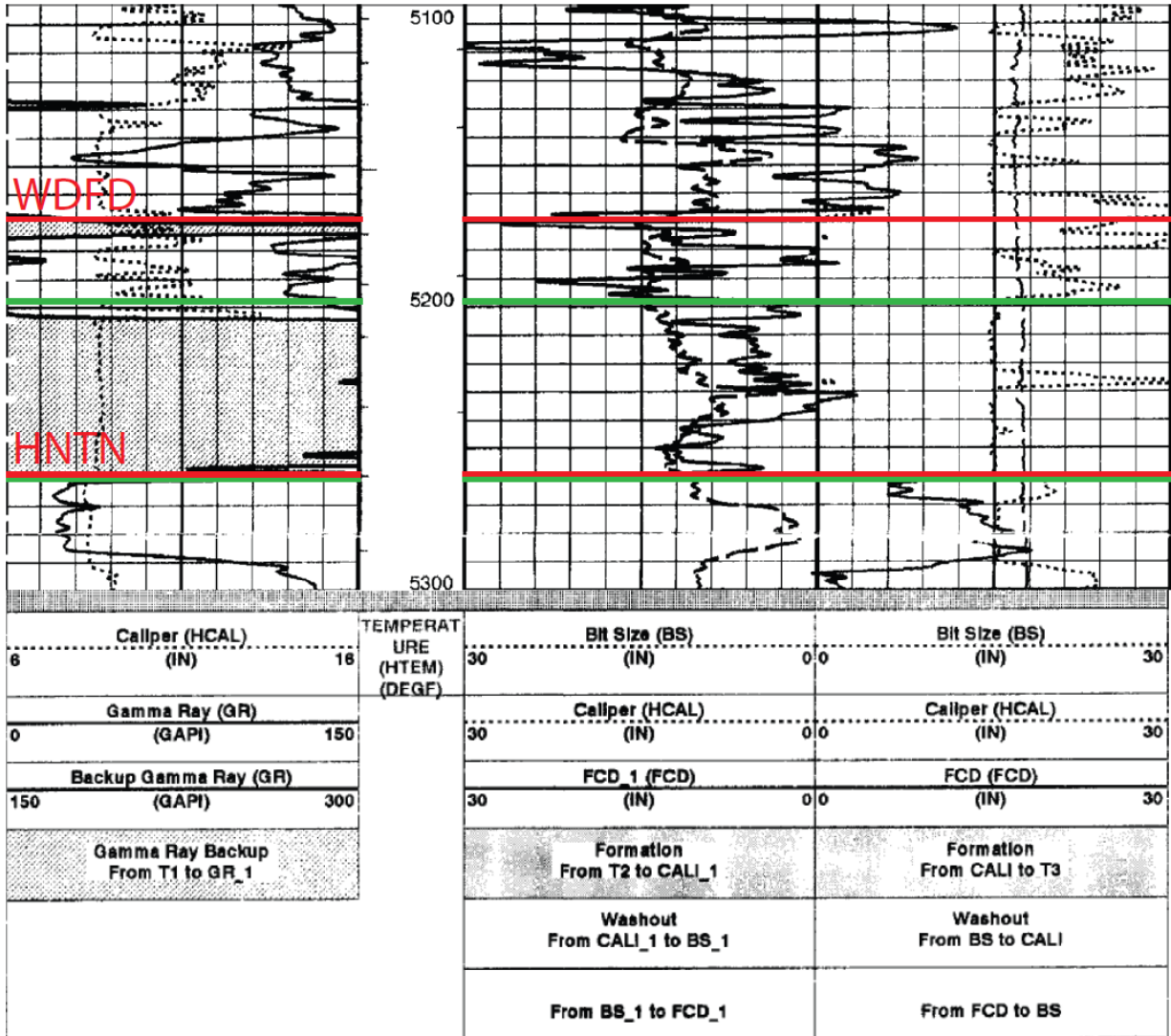
APPENDICES

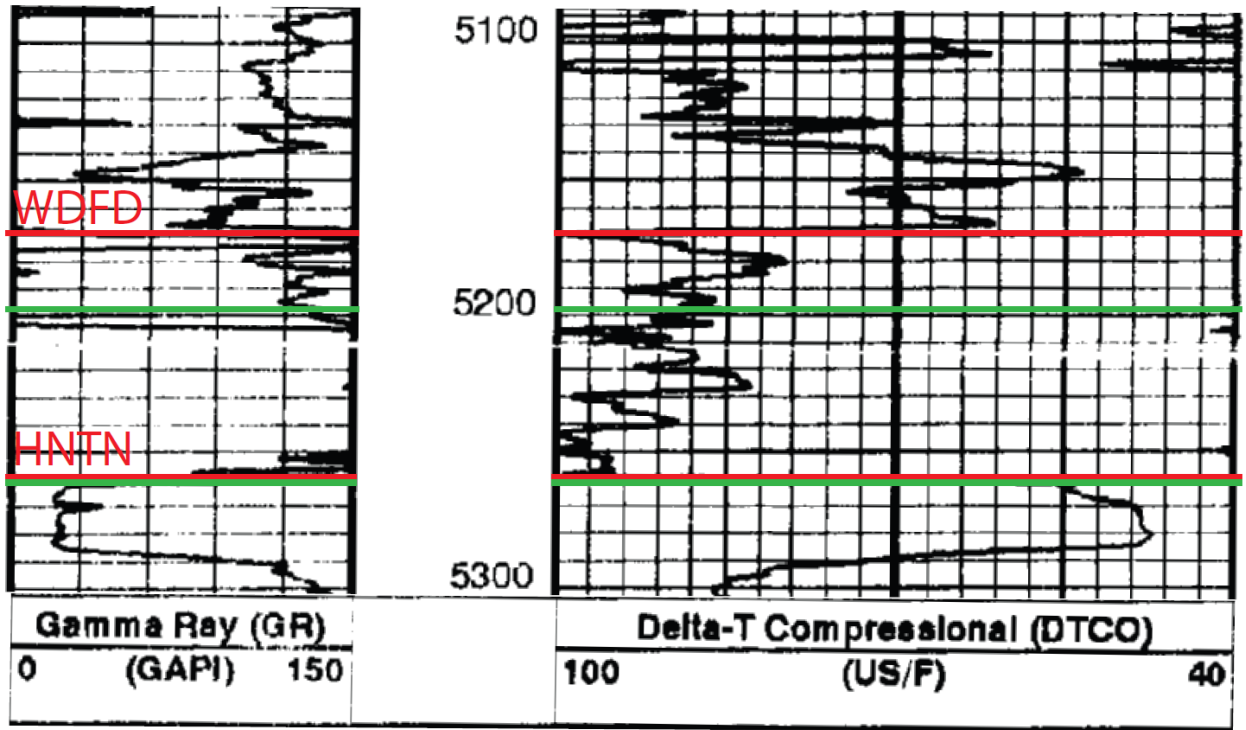Appendix 1: Well Logs from the EOG Smith, B. #31-3 SWD

Gamma Ray and Resistivity Logs; Depth track shows measured depth in feet
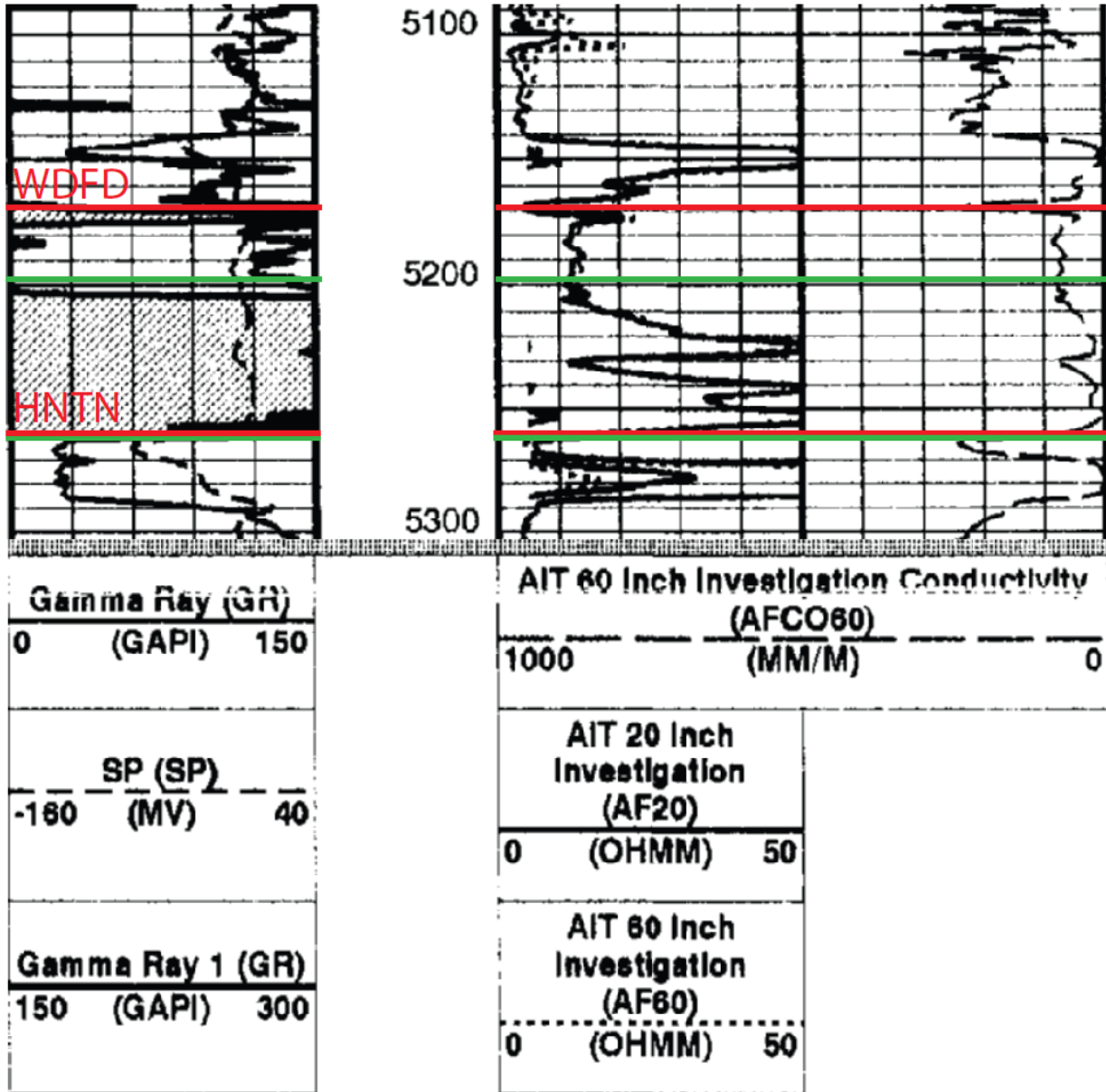
Gamma Ray and Density-Neutron Logs; Depth track shows measured depth in feet

Gamma Ray and Sonic Porosity Logs; Depth track shows measured depth in feet
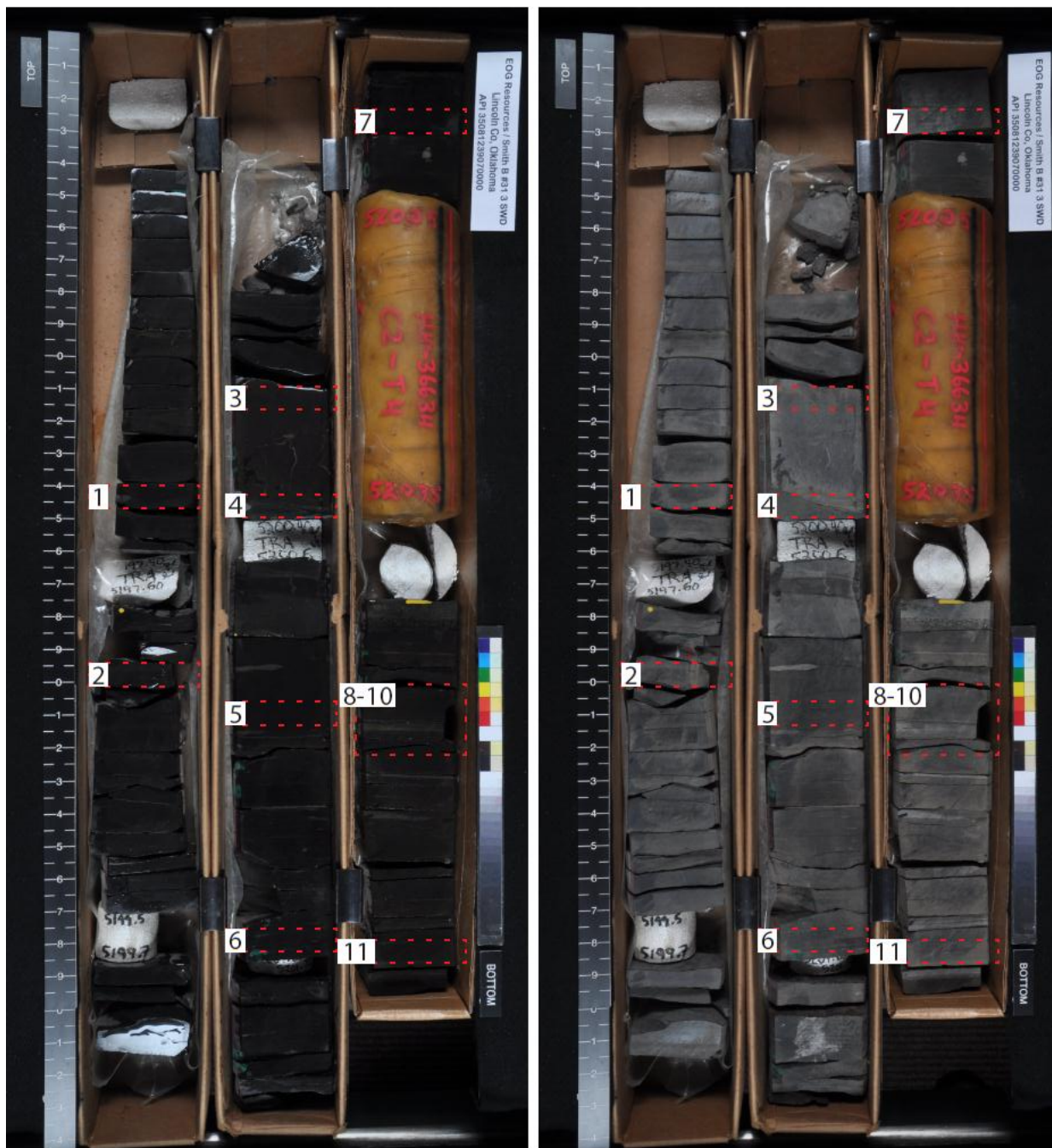
Appendix 2: Whole Core Photographs of the EOG Smith, B. #31-3 SWD Core

Depth Interval: 5196 – 5205 ft (1583.7 – 1586.5 m)

Wet   Dry

Box 1-3: Wet and dry whole core photographs showing a numbered list of the sample locations within this depth interval. See Table 4 for details. Written communication with OPIC, 2012.

Depth Interval: 5205 – 5214 ft (1586.5 – 1589.2 m)

Wet   Dry

Box 4-6: Wet and dry whole core photographs showing a numbered list of the sample locations within this depth interval. See Table 4 for details. Written communication with OPIC, 2012.

Depth Interval: 5214 – 5222 ft (1589.2 – 1591.7 m)

Wet   Dry

Box 7-9: Wet and dry whole core photographs showing a numbered list of the sample locations within this depth interval. See Table 4 for details. Written communication with OPIC, 2012.

Depth Interval: 5222 – 5231 ft (1591.7 – 1594.4 m)

Wet   Dry

Box 10-12: Wet and dry whole core photographs showing a numbered list of the sample locations within this depth interval. See Table 4 for details. Written communication with OPIC, 2012.

Depth Interval: 5231 – 5238.5 ft (1594.4 – 1596.7 m)

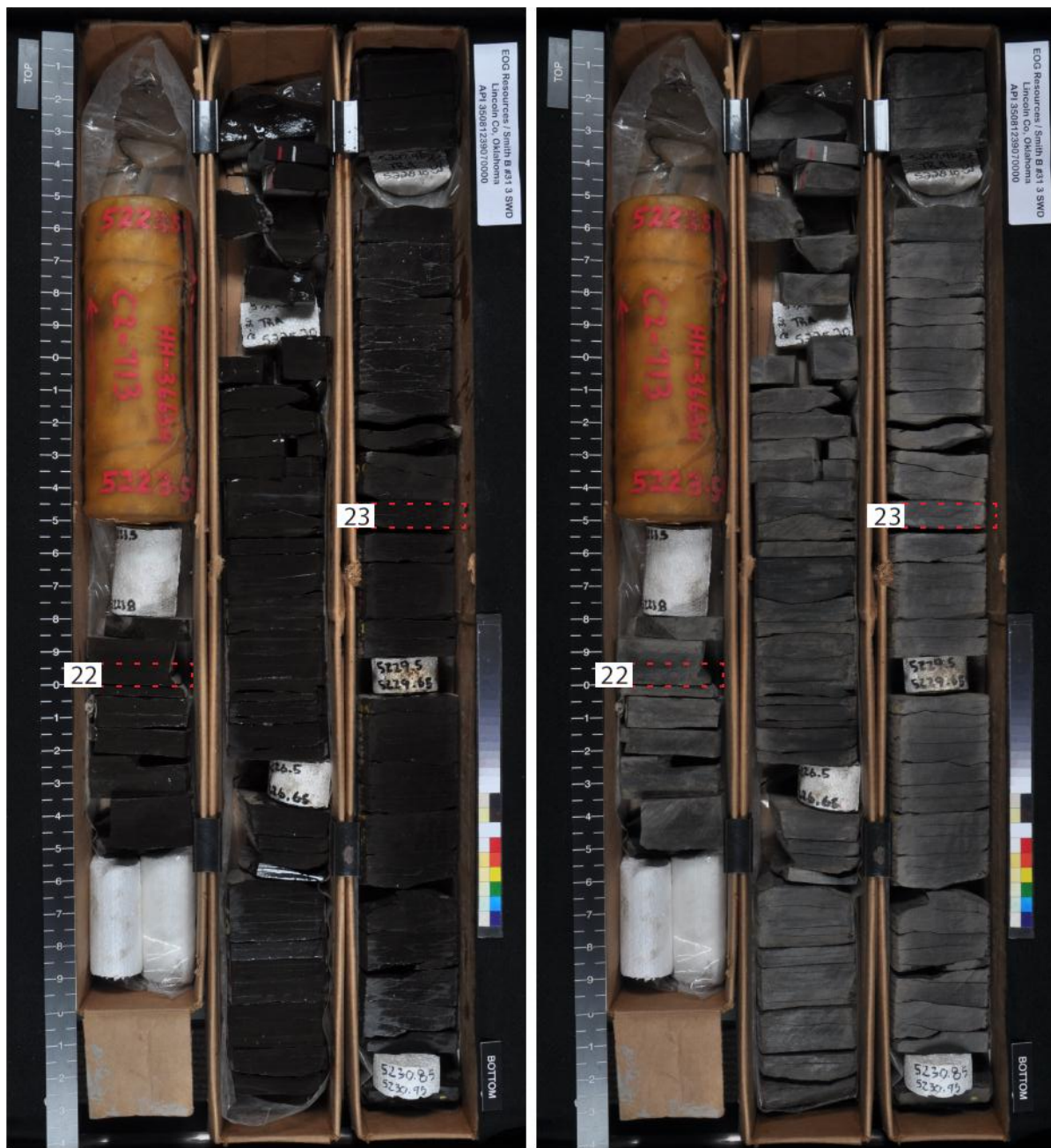Wet   Dry

Box 13-15: Wet and dry whole core photographs showing a numbered list of the sample locations within this depth interval. See Table 4 for details. Written communication with OPIC, 2012.

Depth Interval: 5238.5 – 5247 ft (1596.7 – 1599.3 m)
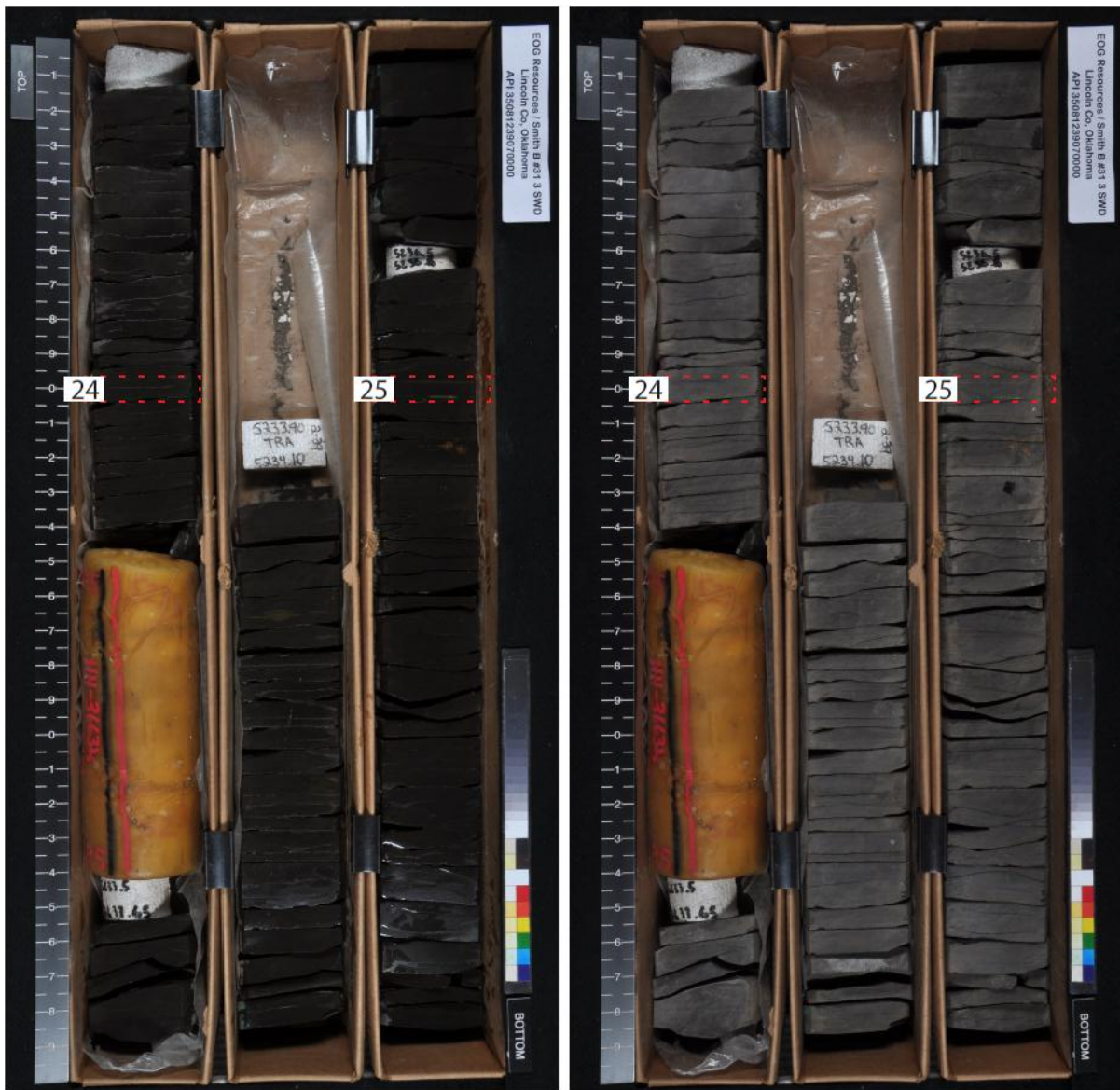
Wet   Dry

Box 16-18: Wet and dry whole core photographs showing a numbered list of the sample locations within this depth interval. See Table 4 for details. Written communication with OPIC, 2012.

Depth Interval: 5247 – 5254 ft (1599.3 – 1601.4 m)

Wet   Dry

Box 19-21: Wet and dry whole core photographs showing a numbered list of the sample locations within this depth interval. See Table 4 for details. Written communication with OPIC, 2012.

Depth Interval: 5254 – 5259.9 ft (1601.4 – 1603.2 m)
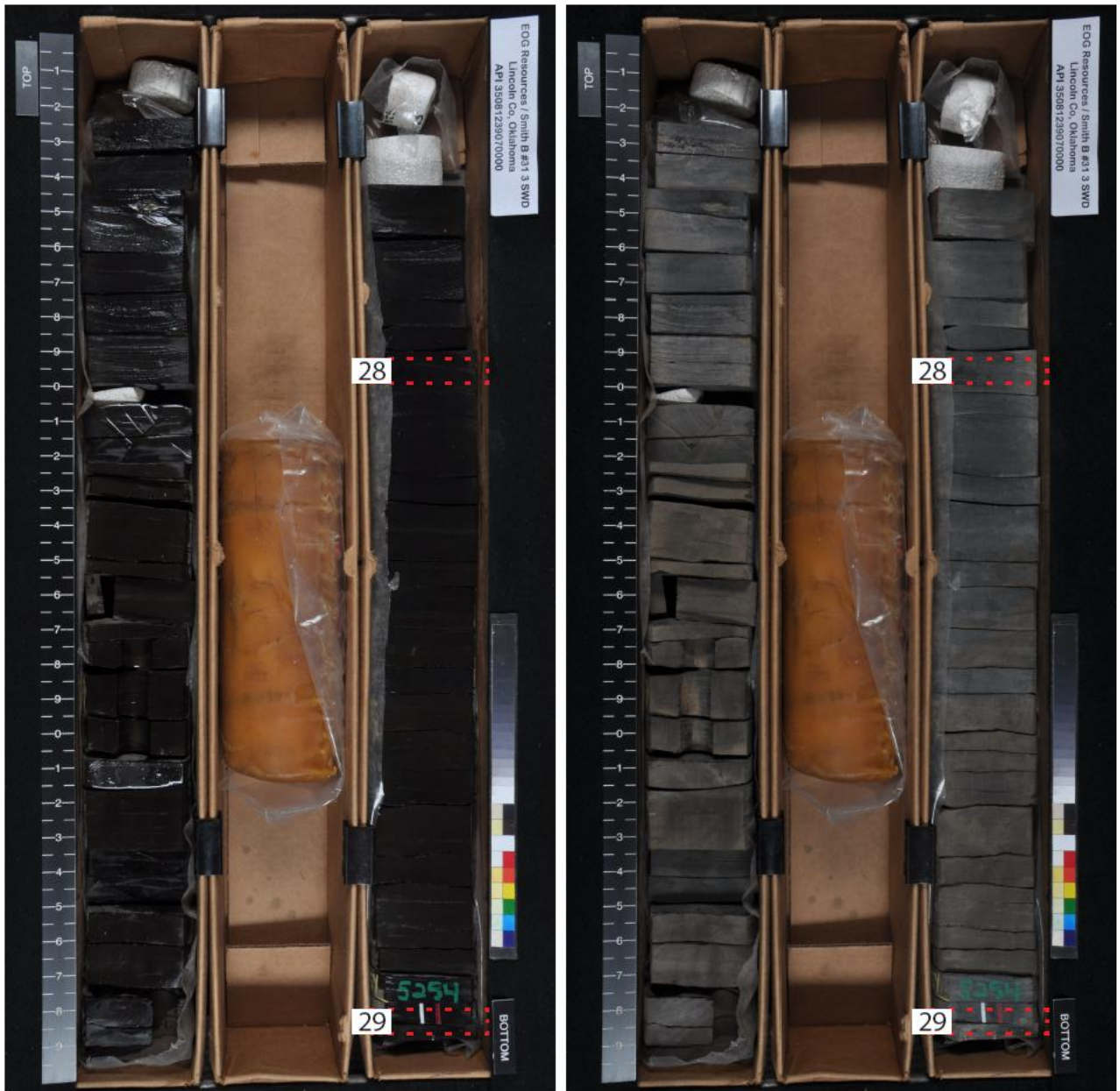
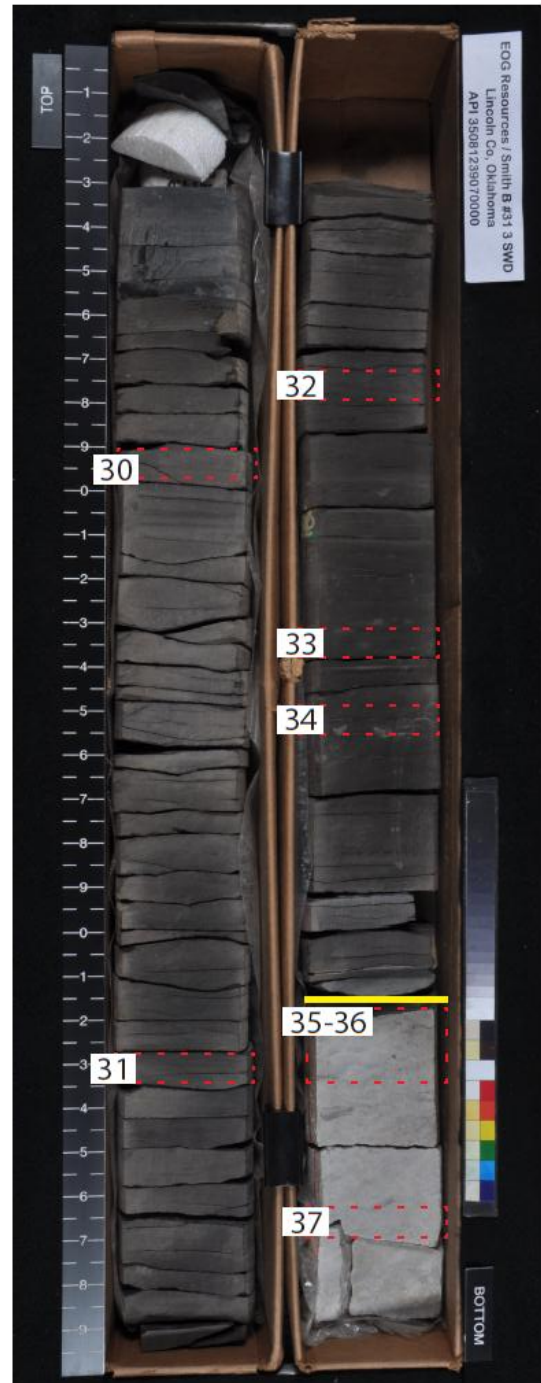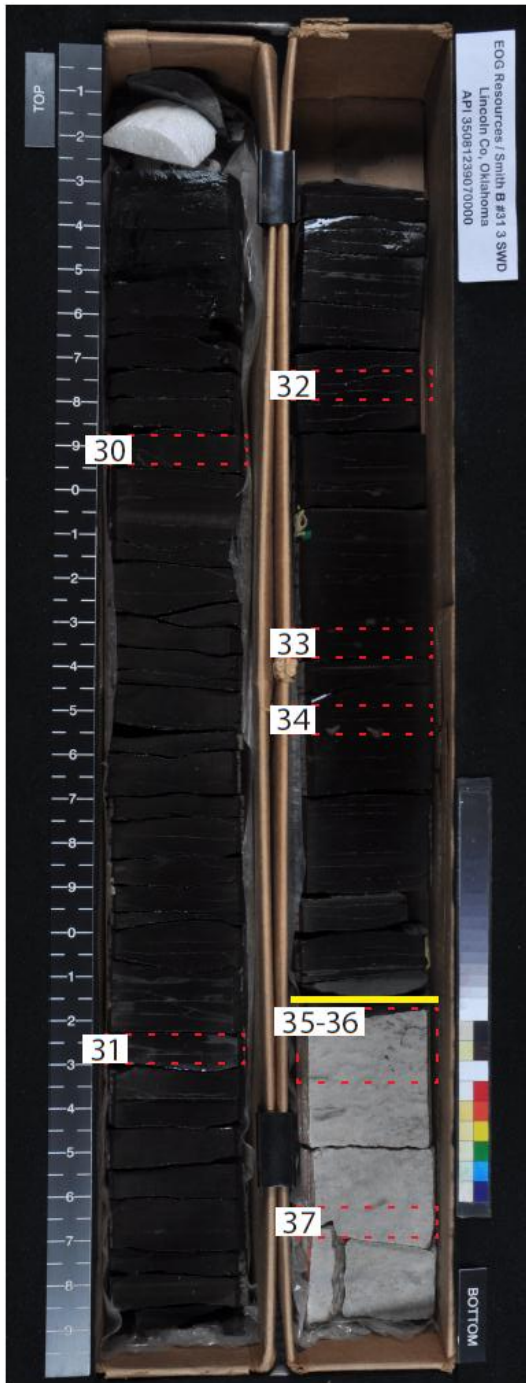Wet   Dry

Box 22-23: Wet and dry whole core photographs showing a numbered list of the sample locations within this depth interval. See Table 4 for details. Written communication with OPIC, 2012.

REFERENCES

Abousleiman, Y.N., Tran, M., Hoang, S., Bobko, C., Ortega, J.A., and Ulm, F.J., 2007, Geomechanics field and lab characterization of Woodford Shale: the next gas play: Society of Petroleum Engineers, Paper SPE 110120, 14 p.

Abousleiman, Y.N., Tran, M., Hoang, S., Ortega, J.A., and Ulm, F.J., 2009, Geomechanics Field Characterization of the Two Prolific U.S. Mid-West Gas Plays with Advanced Wire-Line Logging Tools: SPE paper 124428, SPE Annual Technical Conference, New Orleans, La, Oct. 4th-7th.

Amsden, T.W., 1967, Devonian of the southern midcontinent area, United States, *in* Oswald, D.H., ed., International Symposium on the Devonian System, Alberta Society of Petroleum Geologists, Calgary, Canada, pp. 913-932.

Anderson, E.M., 1951, Dynamics of Faulting and Dike Formation With Application in Britain: 2nd ed., Oliver and Boyd, Edinburgh, 206 p.

Arbenz, J.K., 1989, The Ouachita system, *in* Bally, A.W., and Palmer, A.R., eds., The Geology of North America, Vol. A, The Geology of North America—An Overview: Geological Society of America, pp. 371-396.

Allen, R.W., 2000, Stratigraphy, mountain building and complex geological structures of the Ardmore Basin: Oklahoma Geological Society, Shale Shaker, v. 51, nos. 1-3, pp. 10-21.

Bauernfeind, P.E., 1982, The Misener Sandstone in Portions of Lincoln and Creek Counties, Oklahoma, Oklahoma City Geological Society, Shale Shaker Digest v. 30, pp. 1-30.

Blackford, M.A., 2007, Electrostratigraphy, thickness, and petrophysical evaluation of the Woodford Shale, Arkoma Basin, Oklahoma [M.S. thesis]: Stillwater, Oklahoma State University, 64 p.

Brenneman, M.C., and Smith, P.V., 1958, The chemical relationships between crude oils and their source rocks, *in* Weeks, L.G., ed., Habitat of Oil, American Association of Petroleum Geologists, Tulsa, OK, pp. 818-849.

Burruss, R.C., and Hatch, J.R., 1988, Geochemistry of oils and hydrocarbon source rocks, greater Anadarko Basin: Evidence for multiple sources of oils and long-distance oil migration, *in* Johnson, K.S., ed., Anadarko Basin Symposium, Oklahoma Geological Survey, Circular 90, Norman, OK, 1989, pp. 53-64.

Byerlee, J.D., 1978, Friction of Rocks: Pure & Applied Geophysics, v. 116, pp. 615-626.

Byrnes A.P., and Lawyer, G., 1999, Burial, maturation, and petroleum generation history of the Arkoma basin and Ouachita foldbelt, Oklahoma and Arkansas: Natural Resources Research, v. 8, pp. 3-26.

Cardott, B.J., 1989, Thermal maturation of the Woodford Shale in the Anadarko Basin, *in* Johnson, K.S., ed., Anadarko Basin Symposium, Oklahoma Geological Survey, Circular 90, Norman, OK, 1989, pp. 32-46.

Cargill, J.S., and Shakoor, A., 1990, Evaluation of empirical methods for measuring the uniaxial compressive strength of rock: International Journal of Rock Mechanics and Mining Sciences & Geomechanics Abstracts. v. 27, no. 6, p. 495-503.

Charpentier, R.R., 2001, Cherokee Platform Province (060), U.S. Geological Survey, 1995 National Oil and Gas Resource Assessment Team, Circular 1118, 13 p.

Comer, J.B., 1991, Stratigraphic analysis of the Upper Devonian Woodford Formation, Permian Basin, West Texas and New Mexico: The University of Texas at Austin. Bureau of Economic Geology, Report of Investigations 201, 63 p.

Comer, J.B., 2008, Reservoir characteristics and production potential of the Woodford Shale: World Oil, v. 229, no. 8, pp. 83-89.

Donovan, R.N., Beachamp, W., Ferraro, T., Lajek, D., McConnell, D., Munsil, M., Ragland, D., Sweet, B., and Taylor, D., 1983, Subsidence rates in Oklahoma during the Paleozoic, Oklahoma City Geological Society, Shale Shaker, v. 33, pp. 86-88.

Enderlin, M.B., 2010, A Method for Evaluating the Effects of Confining Stresses and Rock Strength on Fluid Flow Along the Surfaces of Mechanical Discontinuities in Low Permeability Rocks [M.S. Thesis]: Texas Christian University, Fort Worth, 79 p.

Enderlin, M.B., and Alsleben, H., 2012, A Method for Evaluating the Effects of Confining Stresses and Rock Strength on Fluid Flow Along the Surfaces of Mechanical Discontinuities in Low Permeability Rocks, *in* J. Breyer, ed, Shale reservoirs—Giant resources for the 21st century: AAPG Memoir 97, p. 1–21 (in press).

Fertl, W., and Chilingarian, G., 1990, Hydrocarbon resource evaluation in the Woodford Shale using well logs: Journal of Petroleum Science and Engineering, v. 4, pp. 347-357.

Gay, Jr., S.P., 2003, The Nemaha Trend—A System of Compressional Thrust-Fold, Strike-Slip Structural Features in Kansas and Oklahoma, part 2, conclusion, Oklahoma City Geological Society, Shale Shaker, v.54, no.2, pp. 39-49.

Goodman, R.E., 1989, Introduction to rock mechanics: John Wiley & son, New York, 220 p.

Halliburton, 1978, Halliburton Cementing Tables: Halliburton, Duncan, OK, 240 p.

Harlton, B.H., 1951, Faulted fold belts of southern Anadarko basin adjacent to frontal Wichitas: American Association of Petroleum Geologists Bulletin, v. 56, p. 1544-1551.

Heidbach, O., Tingay, M., Barth, A., Reinecker, J., Kurfeb, D., and Müller, B., 2008, The World Stress Map database release 2008 doi:10.1594/GFZ.WSM.Rel2008.

HIS Energy, PI/Dwights, 2009, US Southern Mid-Continent production and well data on CD, Issue 4, v. 9.

Holland, A.A., Keranen, K., and Atekwana, E., 2011, "The Big Quake" - Response and Preliminary Analysis of the November 5, 2011, Magnitude 5.6 Earthquake Sequence, Oklahoma Geological Survey, Oklahoma Geology Notes Vol. 71, No. 4.

Hyne, N.J., 2001, Nontechnical Guide to Petroleum Geology, Exploration, Drilling, and Production: 2nd Edition, PennWell Corporation, Tulsa, OK, 598 p.

Johnson, J.G., Klapper, G., and Sandberg, C.A., 1985, Devonian eustatic fluctuations in Euramerica: Geological Society of America Bulletin, v. 96, no. 5, pp. 567–587.

Johnson, K.S., Amsden, T.W., Denison, R.E., Dutton, S.P., Goldstein, A.G., Rascoe, B. Jr., Sutherland, P.K., and Thompson, D.M., 1989, Geology of the southern Midcontinent: Oklahoma Geological Survey Special Publication 89-2, 53 p.

Johnson, K.S., and Cardott, B.J., 1992, Geologic framework and hydrocarbon source rocks in Oklahoma: Oklahoma Geologic Survey Circular 93, pp. 21-37.

Joseph, L.R., 1987, Subsurface Analysis, "Cherokee" Group (Des Monesian), Portions of Lincoln, Pottawatomi, Seminole and Okfuskee Counties, Oklahoma, Oklahoma City Geological Society, Shale Shaker, v. 37, n. 3, pp. 44-69.

Jusczuk, S.J., 2002, How do the structures of the late Paleozoic Ouachita thrust belt relate to the structures of the southern Oklahoma aulacogen [PhD Dissertation]: Lexington, University of Kentucky, 339 p.

Khaksar, A., Taylor, P.G., Fang, Z., Kayes, T., Salazar, A., and Rahman, K. 2009, Rock Strength from Core and Logs, Where We Stand and Ways to Go. Paper SPE 121972 presented at the EUROPEC/EAGE Conference and Exhibition, Amsterdam, 8–11 June. doi: 10.2118/121972-MS.

Laubach, S.E., Olson, J.O., and Gale, J.F.W., 2004, Are open fractures necessarily aligned with maximum horizontal stress?: Earth and Planetary Science Letters, v. 222, pp.191-195.

Lewan, M.D., Winters, J.C., and McDonald, J.H., 1979, Generation of oil-like pyrolyzates from organic-rich shales, Science, v. 203 no. 4383, pp. 897-899.

Moos, D., and Zoback, M.D., 1990, Utilization of observation of well bore failure to constrain the orientation and magnitude of crustal stresses: application to continental deep sea drilling project and ocean drilling program boreholes: Journal of Geophysical Research 95, p. 9305-9325.

Miall, A.D., and Blakey, R.C., 2008, The Phanerozoic tectonic and sedimentary evolution of North America, *in*, Miall, A.D., ed, Sedimentary Basins of United States and Canada: Elsevier, Amsterdam, pp. 1-29.

Oklahoma Geological Survey, Major Geologic Provinces of Oklahoma. 2008. 1:50 miles. http://www.ogs.ou.edu/pubsscanned/EP9_2-8geol.pdf. Accessed September 9, 2011.

Perry, Jr., W.J., 1995, Arkoma Basin province, *in* Oscarson, S.A. and Clausen, Y.L., eds., USGS Circular 1118, 1995 National Assessment of United States Oil and Gas Resources, Chapter 62.

Ramos, G.G., Chin, L.Y., and Enderlin, M.B., 2008, Up-scaling of Rock Mechanical and Petrophysical Properties from Grain Scale to Log Scale by Point-Load and Wedge Indentation Tests. 42nd U.S. Rock Mechanics Symposium, San Francisco, California. U.S.A

Sierra, R., Tran, M., Abousleiman, Y.N., and Slatt, R.M., 2010, Woodford Shale mechanical properties and impacts of lithofacies: Presented at 44th U.S. Rock Mechanics Symposium, Session 21—Coupled Processes II.

Slatt, R.M., Portas, R., Buckner, N.T., Abousleiman, Y.N., O'Brien, N., Tran, M., Sierra, R., Philp, P., Miceli-Romero, A., Davis, R., and Wawrzyniec, T., 2010, Stratigraphy of the Woodford shale from behind-outcrop drilling, logging, and coring: Norman, University of Oklahoma, p. 483-486.

Sutherland, P.K., 1989, Arkoma Basin: stratigraphy and tectonic framework, *in* Johnson, K.C., Amsden, T.W., Denison, R.E., Dutton, S.P., Goldstein, A.G., Rascoe, B. Jr., Sutherland, P.K., and Thompson, D.M., eds., Geology of the Southern Midcontinent: Oklahoma Geological Survey Special Publication 89-2, pp. 25-34.

United States Geological Survey. 2011. http://earthquake.usgs.gov/earthquakes/recenteqsww/. Accessed November 6, 2011.

Van der Pluijm, B.A., and Marshak, S., 2004, Earth Structure: an introduction to structural geology and tectonics: W. W. Norton & Company, Inc., New York, NY, 656 p.

Weingarten, J.S., and Perkins, T.K., 1995, Prediction of sand production in gas wells: methods and Gulf of Mexico case studies: SPE 24797.

Welte, D.H., Hagemann, H.W., Hollerbach, A., Leythaeuser, D., and Stahl, W., 1975, Correlation between petroleum and source rock, Proceedings of the Ninth World Petroleum Congress, v. 2, pp. 179-191.

Woehrl, B., Wessling, S., Bartetzko, A., Pei, J., and Renner, J., 2010, Comparison of Methods to Derive Rock Mechanical Properties from Formation Evaluation Logs: Presented at 44th U.S. Rock Mechanics Symposium.

Work, P.L., 1975, Digitized well logs can help boost success in exploring shale intervals: Oil and Gas Journal, v. 73, no. 7, pp. 84-88.

Ziegler, P.A., 1989, Evolution of Laurussia: a study in Late Paleozoic plate tectonics: Kluwer Academic Publ., Dordrecht, The Netherlands, 102 p.

Zoback, M.D., 2007, Reservoir Geomechanics: Cambridge University Press, New York, NY, 449 p.

VITA

Personal
Background
Tyler James Hair
Fort Worth, Texas
Born October 22, 1984, KI Sawyer AFB, MI
Son of Richard and Jane Hair
Married to Rachel (Goodwin) Hair, May 1, 2008

Education
Bachelor of Science in Geology, Spanish Minor 2010
Brigham Young University, Provo, UT

Master of Science in Geology, 2012
Texas Christian University, Fort Worth, TX

Experience
Research Assistant, 2008-2010
Brigham Young University Geology Department, Provo, UT

Intern Geologist, 2008-2010
Ridgeland Company, Provo, UT

Teaching Assistant, 2010 -2012
Texas Christian University, Fort Worth, TX

Intern Geologist, 2010-Present
XTO Energy, Fort Worth, TX

Professional
Memberships
American Association of Petroleum Geologists (AAPG)
Fort Worth Geological Society

ABSTRACT

CONSTRUCTING A GEOMECHANICAL MODEL OF THE WOODFORD SHALE,
CHEROKEE PLATFORM, OKLAHOMA, USA
EFFECTS OF CONFINING STRESS AND ROCK STRENGTH ON FLUID FLOW

by Tyler Hair
School of Geology, Energy, and the Environment
Texas Christian University

Thesis Advisor Dr. Helge Alsleben
Committee Members: Milton B. Enderlin, Dr. Nowell Donovan

An equilibrium relationship exists between the rock strength and the magnitude of present-day stresses, such that previously intact rock will break when the stresses acting on a rock diverge beyond the failure point. Reactivation is achieved when a preexisting mechanical discontinuity reaches its failure point. Both stress and strength data are used to construct a geomechanical model to determine the reactivation potential of planar mechanical discontinuities (faults, fractures, bedding planes) in the Woodford Shale. The contemporary stress state of the Cherokee Platform, central Oklahoma, is determined using a stress polygon approach, incorporating Anderson's theory of faulting and available stress data to establish the active fault domain.

A micro-indentation tool is used to estimate the strength of the Woodford Shale from whole core samples through the geometrical attributes (diameter and depth) of a 'dimple' produced by the tool on the rock's surface. The measured dimples are correlated graphically with the unconfined compressive strength and internal friction angle of the Woodford and integrated with contemporary stress data from earthquake focal mechanisms and mapped active faults. Right-lateral strike-slip motion on a deep, unnamed potential splay of the Wilzetta fault is representative of the contemporary stress state of the region. Vertical or near-vertical factures striking ~ 030° from S_{Haz} (~ 077°) are the mechanical discontinuities most likely to be reactivated and allow fluids to flow along their surfaces. This reactivation will occur if the magnitude of pressure sources such as pore pressure or fluid pressure exceeds the reactivation pressure for that fracture surface.